New Journal of Physics
The open access journal at the forefront of physics
Deutsche Physikalische Gesellschaft DPG | IOP Institute of Physics

Decoherence patterns of topological qubits from Majorana modes

Shih-Hao Ho[1,2], Sung-Po Chao[1,2], Chung-Hsien Chou[3] and Feng-Li Lin[4,5]

[1] Physics Division, National Center for Theoretical Science, Hsinchu, 30013, Taiwan
[2] Physics Department, National Tsing Hua University, Hsinchu, 30013, Taiwan
[3] Department of Physics, National Cheng Kung University, Tainan, 70101, Taiwan
[4] Department of Physics, National Taiwan Normal University, Taipei, 11677, Taiwan
E-mail: shho@mx.nthu.edu.tw, spchao@gmail.com, chouch@mail.ncku.edu.tw and linfengli@phy.ntnu.edu.tw

Received 19 July 2014, revised 29 September 2014
Accepted for publication 6 October 2014
Published 24 November 2014

New Journal of Physics **16** (2014) 113062

doi:10.1088/1367-2630/16/11/113062

Abstract

We investigate the decoherence patterns of topological qubits in contact with the environment using a novel way of deriving the open system dynamics, rather than using the Feynman–Vernon approach. Each topological qubit is made up of two Majorana modes of a 1D Kitaev chain. These two Majorana modes interact with the environment in an incoherent way which yields peculiar decoherence patterns of the topological qubit. More specifically, we consider the open system dynamics of topological qubits which are weakly coupled to fermionic/bosonic Ohmic-like environments. We find atypical patterns of quantum decoherence. In contrast to the case for non-topological qubits—which always decohere completely in all Ohmic-like environments—topological qubits decohere completely in Ohmic and sub-Ohmic environments but not in super-Ohmic ones. Moreover, we find that the fermion parities of the topological qubits, though they cannot prevent the qubit states from exhibiting decoherence in sub-Ohmic environments, can prevent thermalization turning the state into a Gibbs state. We also study the cases in which each Majorana mode can couple to different Ohmic-like environments, and the time dependence of concurrence for two topological qubits.

[5] Author to whom any correspondence should be addressed.

Keywords: quantum decoherence, Majorana modes, topological qubits

1. Introduction

Topological quantum computation has been seen as a promising scheme for realizing a quantum computer with robust qubits [1]. The key ingredient for this scheme is based on the anyonic quasiparticles of topologically ordered systems, which are robust against local perturbations due to the underlying topological nature of quantum orders [2]. From the quantum entanglement point of view, these topologically ordered states are endowed with long range entanglement, so collective anyonic excitations are robust against time-like perturbation [3, 4]. That is, the anyons are long range entangled states and so the local perturbations (i.e., local elementary degrees of freedom in the context of condensed matter, or local unitary operations in the context of quantum information) cannot disentangle the anyonic states. There is some evidence of the finding of such intrinsic topologically ordered states in the real world, such as the fractional quantum Hall effect (FQHE). However, anyons with nontrivial anyon statistics, as discussed in [5] for the FQHE, which are the key ingredients for realizing universal quantum computation [1], are not yet observed in experiments. Besides this, the temperature issue for topological order should also be considered in real world experiments[6].

Fortunately, there are new kinds of topologically ordered states, such as topological insulators and superconductors [8–10], which are easier to realize physically. For these systems, some excitations are topologically protected as long as some symmetries such as the time reversal one are preserved. That is, the local perturbations preserving these symmetries cannot disentangle the topological excitations. Among the topological excitations, the most interesting ones are the Majorana modes localized on topological defects, which obey the non-Abelian anyonic statistics [11–13]. The simplest model for realizing such Majorana modes is Kitaev's 1D spineless p-wave superconductor chain model [14–16]. Each on-site fermion d_i can be decomposed into two Majorana modes, γ_{2i-1} and γ_{2i}; that is, $d_i = (\gamma_{2i-1} + \mathrm{i}\gamma_{2i})/2$. By appropriately tuning the model, the Majorana modes at the endpoints of Kitaev's chain can be dangling without pairing with the other nearby Majorana modes to form the usual fermions. Then, these two far separated endpoint Majorana modes can form a topological qubit. The meaning of 'topological' here is twofold: one meaning is that it is made up of Majorana modes γ_1 and γ_{2N} (N denotes the number of regular fermions on the chain) which are topological excitations, and the other meaning is that the topological qubit $d_{\mathrm{topo}} = (\gamma_1 + \gamma_{2N})/2$ is itself nonlocal, i.e., the two Majorana modes are far separated and so cannot combine into a usual fermion. From the quantum information point of view, the topological qubit is EPR-like, as it encodes the quantum state in a nonlocal way. Both features explain its robustness against local perturbations.

As the topological excitations are robust against local perturbations, one might wonder whether the topological qubits are also robust against decoherence when they are considered to be an open system coupling to the non-topological environment. The open system setting is also more realistic when performing quantum computations. As the quantum information is carried

[6] For example, in real work the anyons are in contact with a thermal bath. In this case, the robustness of the topological order has to be reconsidered. For instance, there are results indicating a lack of robustness of the topological order in 2D cases [6], while for higher dimensions there is a robust proposal for self-correcting computation [7]. However, we restrict ourselves to zero-temperature cases in this work.

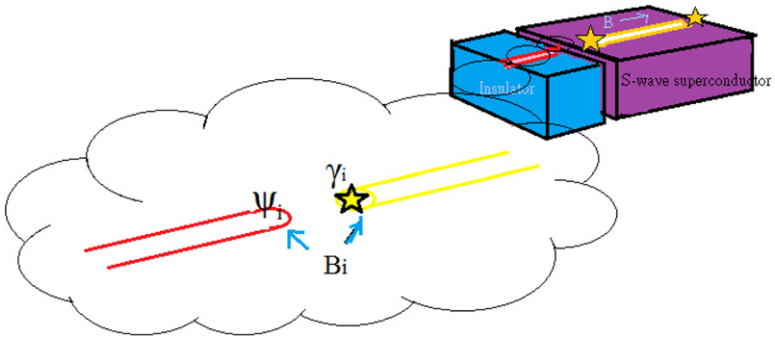

Figure 1. Schematic diagram for Majorana modes coupled to fermionic environments: Majorana modes are generated at the endpoints of some nanowire with strong spin–orbit interaction, placed on top of an s-wave superconductor, and an external magnetic field is applied along the wire axis direction. Each Majorana mode (shown as a gold star) is coupled to a metallic nanowire via a tunnel junction (only one side is shown for simplicity), with the tunneling strength B_i controllable via an external gate voltage. The effective Coulomb interaction of the metallic wire can be tuned via placement at different substrates (shown as the blue region), modifying its dielectric constants.

by physical excitations, the robustness against quantum decoherence implies robustness against local perturbations, but this is not the case the other way around. Even if the excitations are robust against local perturbations, it is still possible for quantum information carried by the topological qubits to leak into the environment. However, as the topological qubit is nonlocal, the way in which it interacts with the environment is quite different from the way in which the usual fermions do, and one would expect atypical quantum decoherence behaviors. This motivates us, in this work, to examine whether the topological qubits are robust against quantum decoherence, and their atypical decoherence patterns.

In fact, it was shown in [21–23] that the topological qubits do decohere, by examining either the relaxation time scale or the behavior of the two-time correlator of Majorana modes[7]. However, to pin down the decoherence patterns, one should directly study the dynamics of the reduced density matrix of the topological qubits. This is what we do in this paper, and the topological qubits do indeed show atypical decoherence patterns. We take one spatial dimensional bosonic or fermionic environment which is universal for (1 + 1) D conformal field theory, such as that of a Luttinger liquid, and has Ohmic-like environmental spectral density, i.e., $\rho_{\rm spec}(\omega) \propto \omega^Q$ with $Q \geqslant 0$. The environment is called Ohmic for $Q = 1$, sub-Ohmic for $Q < 1$ and super-Ohmic for $Q > 1$. For fermionic coupling this is achieved by placing a metallic nanowire close to the Majorana endpoint as shown in figure 1. The Coulomb interaction within

[7] The single topological qubit considered in [21–23] is made by the parity even sector of four Majorana modes, instead of the two Majorana modes considered in this work. This is because, by the superselection rule, one cannot observe the relative phase in the linear superposition of two degenerate eigenstates of a parity operator. In this work, we bypass the superselection rule by preparing the general (parity-broken) initial state induced by the parity-violating operator. This can be done either by shortening the Kitaev chain (such that the tunneling strength is increasing) or by turning on the parity-breaking probe–environment operators (recall that the distance between two Majorana modes of a single qubit, especially in the ring case, is very small in our setup). Once the general initial states are prepared, our dynamics follows. On the other hand, a qubit made up of an even sector of four Majorana modes will be a special case of our two-qubit cases, so our conclusion also holds in such a reduced case.

the wire can be tuned by choosing a different insulating substrate or gating, and the low energy excitation of the wire is deemed to provide a Luttinger liquid.

We also assume the coupling between the Majorana modes and the environment to be weak so that the Gaussian approximation holds good. This also ensures that the influence of the Ohmic-like environment on the bulk of the Kitaev chain is irrelevant, so the robustness of the Majorana modes is protected. We find that the topological qubits decohere completely in the Ohmic and sub-Ohmic environments but not in the super-Ohmic environments; i.e., they do not relax to the Gibbs state or pointer state. Thus, for the super-Ohmic environments one may be able to distill the purity or concurrence of the resultant state of topological qubits by appropriate quantum information manipulations. This feature is atypical as compared to what is found for the decoherence patterns of the non-topological qubits studied in [27, 28, 44], where the local qubits always decohere in all Ohmic-like environments if the probe–environment coupling is weak. Thus, we conclude that the topological nature does protect the topological qubits from decoherence to some extent.

We organize our paper as follows. In the next section we briefly introduce the setup of topological qubits made up of Majorana modes interacting with the environment via coupling to either fermionic or bosonic operators. We then develop our interaction picture formalism for deriving the open system dynamics of the topological qubits. In section 3 we study the decoherence patterns of single and double topological qubits weakly coupled to Ohmic-like environments. We obtain the explicit form of the reduced density matrix for the single topological qubit in order to see the decoherence patterns. For two topological qubits, various results concerning the robustness against complete decoherence are fully revealed both analytically and numerically. Finally, we conclude our paper in section 4. Various technical details concerning the real time Green functions and the explicit forms of the reduced density matrices are given in the Appendices.

2. Dynamics of the open system for Majorana qubits

In this section we consider an open system of topological qubits made up of Majorana modes and study the dynamics of its reduced density matrix. The peculiar features of Majorana modes, such as them obeying the Clifford algebra, make the consideration of their decoherence far simpler than the case for the usual simple harmonic oscillator probe. As we show below, the reduced dynamics of this open system obtained by integrating out the environment can be obtained in a closed form when formulating the formalism in the interaction picture. This is in contrast to the case for the usual Feynman–Vernon formulation for non-topological qubits [43, 44], for which one needs to numerically solve the Langevin-like equation involved.

2.1. The open system for Majorana modes

The system considered in this paper is described by the following Hamiltonian:

$$H = \hat{H}_0 + \hat{V} = \hat{H}_{\mathcal{P}} + \hat{H}_{\mathcal{E}} + \hat{V} \tag{1}$$

where $\hat{H}_0$ is the free Hamiltonian consisting of $\hat{H}_{\mathcal{P}}$ for the probe $\mathcal{P}$ and $\hat{H}_{\mathcal{E}}$ for the environment $\mathcal{E}$, and $\hat{V}$ is the interaction between $\mathcal{P}$ and $\mathcal{E}$. We also assume that $[\hat{H}_{\mathcal{P}}, \hat{H}_{\mathcal{E}}] = 0$.

Here the probe consists of a bunch of Majorana modes localized at the ends of some quantum wires ([14]; see also [17, 18] for experimental proposals). We denote these localized

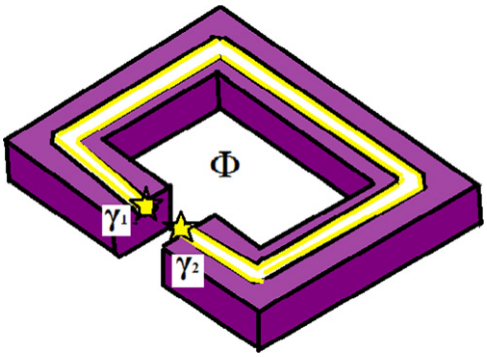

Figure 2. Schematic diagram for two Majorana modes coupled with a bosonic environment. The two Majorana modes are located at the endpoints of a ring with a small gap in between. The pair of Majorana modes γ_1 and γ_2 interact with some effective environmental bosonic operator locally. The frequency dependence in the bosonic environment can in principle be generated by an external time-dependent magnetic flux Φ; this is similar to the proposal in [19].

Majorana modes as γ_a, with $a = 1, 2, \ldots$; they have the following properties:

$$\gamma_a^\dagger = \gamma_a, \qquad \{\gamma_a, \gamma_b\} = 2\delta_{ab}. \tag{2}$$

On the other hand, the dynamics of the environment is dictated by $\hat{H}_\mathcal{E}$ whose elementary constituents can be thought of as electrons or holes. Due to the aforementioned peculiar properties of the γ_as, the generic interaction Hamiltonian takes the form

$$\hat{V} = \sum_a B_a \gamma_a \mathcal{O}_a + \sum_{a>b} B_{ab} \gamma_a \gamma_b \mathcal{O}_{ab} + \cdots, \tag{3}$$

where the B_as and B_{ab}s are real coupling constants, and the $\mathcal{O}_a$s and $\mathcal{O}_{ab}$s are composite operators constructed from the electrons' creation and annihilation operators $\psi_\alpha^\dagger$ and ψ_α, with $\alpha = a, b$ labeling the electrons' bath and spin indices. For the tunneling junction shown in figure 1, $\mathcal{O}_a = \psi_a^\dagger - \psi_a$. The $\cdots$ denotes the higher order terms involving greater numbers of Majorana modes, which however are not considered in this paper. Moreover, note that

$$\mathcal{O}_a^\dagger = -\mathcal{O}_a, \qquad \mathcal{O}_{ab}^\dagger = -\mathcal{O}_{ab}. \tag{4}$$

These expressions follow from the Hermitian condition for the full Hamiltonian.

As the Majorana modes could be spatially separated, the second term in equation (3) could be nonlocal, i.e., we could have $\gamma_a \gamma_b \mathcal{O}_{ab} := \gamma_a(\mathbf{x}) \mathcal{O}_{ab}(\mathbf{x}, \mathbf{y}) \gamma_b(\mathbf{y})$. For simplicity, in this work we only consider the local interactions. In such cases, the locality for the two localized Majorana modes can be arranged either as in figure 1, for neighboring wires, or as in figure 2, for a ring with a small gap.

The density matrix $\hat{\rho}(t)$ for the whole system in the Schrödinger picture evolves as

$$\hat{\rho}(t) = |\psi(t)\rangle\langle\psi(t)| = \mathrm{e}^{-\mathrm{i}\hat{H}t}\, \hat{\rho}_0\, \mathrm{e}^{\mathrm{i}\hat{H}t}, \tag{5}$$

where $\hat{\rho}_0 \equiv \hat{\rho}(t = 0)$. We assume the direct product structure for $\hat{\rho}_0$, i.e.,

$$\hat{\rho}_0 = \hat{\rho}_\mathcal{P} \otimes \hat{\rho}_\mathcal{E}. \tag{6}$$

In general, $\hat{V}$ mixes the probe's and the environment's degrees of freedom such that $[\hat{H}_0, \hat{V}] \neq 0$. This prevents further simplification when evaluating the reduced density matrix for probe $\mathcal{P}$, i.e.,

$$\hat{\rho}_{\rm r}(t) = {\rm Tr}_{\mathcal{E}}\, {\rm e}^{-{\rm i}\hat{H}t}\, \hat{\rho}_0\, {\rm e}^{{\rm i}\hat{H}t}, \tag{7}$$

where ${\rm Tr}_{\mathcal{E}}$ indicates taking the trace over the Hilbert space of environment $\mathcal{E}$. We rewrite equation (7) as

$$\begin{aligned}\langle i|\, \hat{\rho}_{\rm r}(t)|\, j\rangle = & \sum_{m_+,m_-,K,L_+,L_-} \langle i,\, K|\, {\rm e}^{-{\rm i}\hat{H}t}\, \big|m_+,\, L_+\big\rangle \\ & \times \big\langle m_+,\, L_+\big|\, \hat{\rho}_0\, \big|m_-,\, L_-\big\rangle\, \big\langle m_-,\, L_-\big|\, {\rm e}^{{\rm i}\hat{H}t}\, |j,\, K\rangle,\end{aligned} \tag{8}$$

where the lower case letters such as i, j, $m_\pm$ are labels for the probe's state space, and the upper case ones such as K, $L_\pm$ are ones for the environment's state space. Although we use the notation with discrete labels, the generalization to the continuum is straightforward.

The first and third factors in equation (8) can be understood as the Schwinger–Keldysh Green functions [29, 30] on the forward (labeled with the subscript '+') and backward (labeled with the subscript '−') real time Keldysh contours [30], respectively. Due to the fact that $[\hat{H}_0, \hat{V}] \neq 0$, it is usually difficult to simplify these Green functions further. The standard practice in deriving the dynamics of the reduced density matrix is to adopt Feynman–Vernon formalism [31–33], by integrating out the environment in the path-integral formulation and obtaining a real time effective theory (the so-called 'influence functional') for the probe.

2.2. The interaction picture formulation

The Feynman–Vernon formalism usually involves solving a Langevin-like equation with a complicated nonlocal kernel in order to explicitly obtain $\hat{\rho}_{\rm r}(t)$. This usually needs careful numerical computations. Here we show that for a probe composed of Majorana modes, even with $[\hat{H}_0, \hat{V}] \neq 0$, the calculations needed for obtaining $\hat{\rho}_{\rm r}(t)$ in the formulation of the interaction picture are greatly simplified, with no need for introducing a path integral and solving a Langevin-like equation. We elaborate on this formulation as follows.

The full density matrix in the interaction picture is

$$\begin{aligned}\hat{\rho}_I(t) &\equiv {\rm e}^{{\rm i}\hat{H}_0 t}\hat{\rho}(t){\rm e}^{-{\rm i}\hat{H}_0 t} \\ &= {\rm e}^{{\rm i}\hat{H}_0 t}{\rm e}^{-{\rm i}\hat{H}t}\hat{\rho}_0{\rm e}^{{\rm i}\hat{H}t}{\rm e}^{-{\rm i}\hat{H}_0 t} = U(t)\hat{\rho}_0 U^\dagger(t),\end{aligned} \tag{9a}$$

where the evolution operator $U(t) \equiv {\rm e}^{{\rm i}\hat{H}_0 t}{\rm e}^{-{\rm i}\hat{H}t}$. The evolution operator satisfies the Schrödinger equation

$${\rm i}\,\frac{{\rm d}}{{\rm d}t}U(t) = \hat{V}_I(t)U(t), \tag{9b}$$

where

$$\hat{V}_I(t) \equiv {\rm e}^{{\rm i}\hat{H}_0 t}\ \hat{V}\ {\rm e}^{-{\rm i}\hat{H}_0 t}. \tag{9c}$$

For the interaction equation (3) considered here, we have

$$\hat{V}_I(t) = \sum_a B_a \gamma_a(t)\mathcal{O}_a(t) + \sum_{a<b} B_{ab}\gamma_a\gamma_b(t)\mathcal{O}_{ab}(t), \tag{9d}$$

where

$$\mathcal{O}_{\mathcal{P}}(t) = \mathrm{e}^{-\mathrm{i}H_{\mathcal{P}}t}\mathcal{O}_{\mathcal{P}}\mathrm{e}^{\mathrm{i}H_{\mathcal{P}}t},\ \mathcal{O}_{\mathcal{E}}(t) = \mathrm{e}^{-\mathrm{i}H_{\mathcal{E}}t}\mathcal{O}_{\mathcal{E}}\mathrm{e}^{\mathrm{i}H_{\mathcal{E}}t}, \tag{9e}$$

with $\mathcal{O}_{\mathcal{P}} = \gamma_a$ or $\gamma_a\gamma_b$, and $\mathcal{O}_{\mathcal{E}} = \mathcal{O}_a$ or $\mathcal{O}_{ab}$.

We then solve equation (9*b*) to arrive at

$$U(t) = \mathrm{T}\,\mathrm{e}^{-\mathrm{i}\int^t \mathrm{d}\tau\ \hat{V}_I(\tau)}. \tag{9f}$$

Here T is the time-ordering operator on the forward Keldysh contour. We also denote the time-ordering operator on the backward Keldysh contour as $\tilde{\mathrm{T}}$, such that

$$U^\dagger(t) = \tilde{\mathrm{T}}\,\mathrm{e}^{\mathrm{i}\int^t \mathrm{d}\tau\ \hat{V}_I(\tau)}. \tag{9g}$$

It is easy to check that $\hat{\rho}_I(t)$ satisfies the following equation of motion, i.e., the Schrödinger equation for the density matrix:

$$\frac{\mathrm{d}}{\mathrm{d}t}\hat{\rho}_I(t) = -\mathrm{i}\Big[\hat{V}_I(t),\, \hat{\rho}_I(t)\Big]. \tag{9h}$$

On the basis of the interaction picture, it is easy to see that the reduced density matrix for probe $\mathcal{P}$ can be further simplified as follows:

$$\begin{aligned}\hat{\rho}_{\mathrm{r}}(t) &= \mathrm{e}^{-\mathrm{i}\hat{H}_{\mathcal{P}}t}\Big(\mathrm{Tr}_{\mathcal{E}}\,\mathrm{e}^{-\mathrm{i}\hat{H}_{\mathcal{E}}t}\hat{\rho}_I(t)\mathrm{e}^{\mathrm{i}\hat{H}_{\mathcal{E}}t}\Big)\mathrm{e}^{\mathrm{i}\hat{H}_{\mathcal{P}}t},\\ &= \mathrm{e}^{-\mathrm{i}\hat{H}_{\mathcal{P}}t}\Big(\mathrm{Tr}_{\mathcal{E}}\,\hat{\rho}_I(t)\Big)\mathrm{e}^{\mathrm{i}\hat{H}_{\mathcal{P}}t},\\ &= \mathrm{e}^{-\mathrm{i}\hat{H}_{\mathcal{P}}t}\Big(\mathrm{Tr}_{\mathcal{E}}\,U(t)\hat{\rho}_0 U^\dagger(t)\Big)\mathrm{e}^{\mathrm{i}\hat{H}_{\mathcal{P}}t}.\end{aligned} \tag{10}$$

In the first line we have used the fact that $[\hat{H}_{\mathcal{P}}, \hat{H}_{\mathcal{E}}] = 0$, and in the second line we simply use the cyclic property of the trace operation and $\mathrm{e}^{-\mathrm{i}\hat{H}_{\mathcal{E}}t}\mathrm{e}^{\mathrm{i}\hat{H}_{\mathcal{E}}t} = 1$. In the final expression, the $\hat{H}_{\mathcal{E}}$ dependence is implicitly hidden in $\mathcal{O}_{\mathcal{E}}(t)$.

2.3. The reduced density matrix for the Majorana probe

As these Majorana modes used for the qubits are zero-energy modes, we have

$$\hat{H}_{\mathcal{P}} = 0 \tag{11}$$

and thus $\mathcal{O}_{\mathcal{P}}(t) = \mathcal{O}_{\mathcal{P}}$, i.e., $\gamma_a(t) = \gamma_a$, etc.

To obtain the simple analytic reduced dynamics, we consider the interaction Hamiltonian in which the individual terms in equation (3) commute with each other. For example, we cannot have both $\gamma_1\mathcal{O}_1$ and $\gamma_1\gamma_2\mathcal{O}_{12}$, or both $\gamma_1\gamma_2\mathcal{O}_{12}$ and $\gamma_2\gamma_3\mathcal{O}_{23}$. Otherwise, we would not have the closed form for the reduced dynamics. Although this constraint looks artificial just for simplifying the derivation, it can be naturally realized once the shape of the nanowire is given, as the Majorana modes are confined to the endpoints of the wire. For example, as γ_1 and γ_2 are located at the two ends of the nanowire, we can only have $\gamma_i\mathcal{O}_i$ and not $\gamma_1\gamma_2\mathcal{O}_{12}$ for a straight

wire. On the other hand, for a ring wire with an extremely narrow gap, as in figure 2, it is natural to just have $\gamma_1\gamma_2\mathcal{O}_{12}$ and not $\gamma_i\mathcal{O}_i$.

Given the above constraint, the evolution operator $U(t)$ can be decomposed as

$$\begin{aligned} U(t) &:= \mathrm{T}\,\Pi_M \mathrm{e}^{-\mathrm{i}\Gamma_M \mathbf{O}_M(t)} \\ &= \mathrm{T}\,\Pi_a \mathrm{e}^{-\mathrm{i}B_a\gamma_a \int^t \mathrm{d}\tau\, \mathcal{O}_a(\tau)}\ \Pi_{a<b}\ \mathrm{e}^{-\mathrm{i}B_{ab}\gamma_a\gamma_b \int^t \mathrm{d}\tau\, \mathcal{O}_{ab}(\tau)}. \end{aligned} \tag{12}$$

Here we combine the set of operator indices a and ab into a unified symbol M such that $\Gamma_M = \gamma_a$ or $\gamma_a\gamma_b$, and so on. Moreover, for simplicity we have denoted $B_M \int^t \mathrm{d}\tau\, \mathcal{O}_M(\tau)$ as $\mathbf{O}_M(t)$, with the time-ordering being taken care of.

Using the properties given in equation (2) for the γ_as, each factor in equation (12) is further simplified, namely,

$$\mathrm{T}\,\mathrm{e}^{-\mathrm{i}\Gamma_M \mathbf{O}_M(t)} = \mathrm{T}\left[\cosh \mathbf{O}_M(t) - \mathrm{i}\Gamma_M \sinh \mathbf{O}_M(t)\right]. \tag{13}$$

Note that in the above we have used the fact that the $\mathbf{O}_a$s are fermionic operators and the $\mathbf{O}_{ab}$s are bosonic ones. Thus the time-ordered evolution matrix is

$$U(t) = \mathrm{T}\,\Pi_M\left[\cosh \mathbf{O}_M(t) - \mathrm{i}\Gamma_M \sinh \mathbf{O}_M(t)\right]. \tag{14}$$

Similarly, the anti-time-ordered one is

$$U^\dagger(t) = \tilde{\mathrm{T}}\,\Pi_M\left[\cosh \mathbf{O}_M(t) + \mathrm{i}\Gamma_M \sinh \mathbf{O}_M(t)\right]. \tag{15}$$

We further simplify equation (10) by using the fact that $\mathrm{Tr}_\mathcal{E}(\hat{\rho}_\mathcal{E}\mathcal{O}_\mathcal{E}) = 0$ if $\mathcal{O}_\mathcal{E}$ is a fermionic operator of the environmental theory, i.e.,

$$\left\langle \mathcal{O}_\mathcal{E} \right\rangle_\mathcal{E} = 0 \quad \text{if } \mathcal{O}_\mathcal{E} \text{ is fermionic.} \tag{16}$$

Thus, the reduced density matrix should take the form

$$\begin{aligned} \hat{\rho}_\mathrm{r}(t) = \sum_{\{m\},\{m'\}} & \mathrm{e}^{\mathrm{i}\phi_{m,m'}}\left[\Pi_{\{m\}}\mathcal{G}_m\hat{\rho}_\mathcal{P}\Pi_{\{m'\}}\mathcal{G}_{m'}\right]_+ \\ & \times \left\langle \left[\tilde{\mathrm{T}}\,\Pi_{\{m'\}}\mathcal{H}_{m'}(t)\ \mathrm{T}\,\Pi_{\{m\}}\mathcal{H}_m(t)\right]_+ \right\rangle_\mathcal{E}, \end{aligned} \tag{17}$$

where $[\cdots]_+$ denotes that the operator $\cdots$ is of even fermion parity, $\mathcal{H}_m(t)$ is either $\cosh \mathbf{O}_M(t)$ or $\sinh \mathbf{O}_M(t)$, and $\mathcal{G}_m$ in $\Pi_{\{m\}}\mathcal{G}_m$ is 1 if $\mathcal{H}_m(t) = \cosh \mathbf{O}_M(t)$; otherwise it is Γ_M. The phase factor $\mathrm{e}^{\mathrm{i}\phi_{m,m'}} = \pm 1, \pm\mathrm{i}$ is determined by the relative ordering of the fermionic operators, and $\sum_{\{m\},\{m'\}}$ runs over all possible sets of even fermion parity terms in the binomial expansion of $U\hat{\rho}_0 U^\dagger$. Here, we have used shorthand notation for the real time Green function, i.e.,

$$\begin{aligned} &\left\langle \left[\tilde{\mathrm{T}}\,\Pi_{\{m'\}}\mathcal{H}_{m'}(t)\ \mathrm{T}\,\Pi_{\{m\}}\mathcal{H}_m(t)\right]_+ \right\rangle_\mathcal{E} \\ &\quad := \mathrm{Tr}_\mathcal{E}\left[\mathrm{T}\,\Pi_{\{m\}}\mathcal{H}_m(t)\hat{\rho}_\mathcal{E}\tilde{\mathrm{T}}\,\Pi_{\{m'\}}\mathcal{H}_{m'}(t)\right]_+. \end{aligned} \tag{18}$$

Due to the locality of the Majorana modes, we assume that the environments for different channels are independent, i.e.,

$$\left\langle \mathcal{O}_{\mathcal{E}}\tilde{\mathcal{O}}_{\mathcal{E}}\right\rangle_{\mathcal{E}}=0,\qquad \text{if}\quad \mathcal{O}_{\mathcal{E}}\neq\tilde{\mathcal{O}}_{\mathcal{E}}. \tag{19}$$

In such a case, equation (17) is further simplified as

$$\begin{aligned}\hat{\rho}_{\mathrm{T}}(t)=&\sum_{\{m\}}(-1)^{\frac{1}{2}m_{\mathrm{F}}(m_{\mathrm{F}}-1)}\left[\Pi_{\{m\}}\mathcal{G}_m\hat{\rho}_{\mathcal{P}}\Pi_{\{m\}}\mathcal{G}_m\right]_+\\&\times\left[\Pi_{\{m\}}\left\langle\tilde{\mathrm{T}}\,\mathcal{H}_m(t)\;\mathrm{T}\,\mathcal{H}_m(t)\right\rangle_{\mathcal{E}}\right]_+,\end{aligned} \tag{20}$$

where m_{F} is the number of fermionic operators in $\Pi_{\{m\}}\mathcal{H}_m$, i.e., the cosh $\mathcal{O}_a$s, cosh $\mathcal{O}_{ab}$s and sinh $\mathcal{O}_{ab}$s are bosonic but the sinh $\mathcal{O}_a$s are fermionic. Here $\sum_{\{m\}}$ runs over all the binomial terms of $\Pi_M(\cosh\mathbf{O}_M+\sinh\mathbf{O}_M)$ for $\Pi_{\{m\}}\mathcal{H}_m$, and $\mathcal{G}_m$ in $\Pi_{\{m\}}\mathcal{G}_m$ is 1 if $\mathcal{H}_m(t)=\cosh\mathbf{O}_M(t)$; otherwise it is Γ_M. Again, due to equation (16) those nonvanishing terms are of even fermion parity.

Before we consider the specific cases to obtain the explicit dynamics of $\hat{\rho}_{\mathrm{T}}(t)$, three important remarks about arriving at the form of equation (20) should be made:

- As both the probe and the environment factors in equation (20) are of even fermion parity, and are thus bosonic and commute with each other, the total Hilbert space can be cast into the form of direct products of that for the probe and that for the environment, i.e., equation (6). Thus, we can evaluate the first factor of the Majorana modes in terms of the finite dimensional representation of the Clifford algebra $\{\gamma_a,\gamma_b\}=2\delta_{ab}$.
- Even if $\mathcal{O}_a$ is a fermionic operator, we should treat it as a bosonic operator when evaluating its corresponding real time Green function in equation (20) [21]. This can be understood from the fact that γ_a always accompanies $\mathcal{O}_a$ as indicated in equation (13), so the minus sign arising from the switching of the $\mathcal{O}_a$s as required by the time-ordering is cancelled by the analogous minus sign for γ_a. The latter minus sign is implicit, as we set $\hat{H}_{\mathcal{P}}=0$. To make this explicit, we assume that $\hat{H}_{\mathcal{P}}\neq 0$; then

$$\begin{aligned}&\left\langle\mathrm{T_C}\,\mathcal{O}_a(t)\gamma_a(t)\gamma_a(t')\mathcal{O}_a(t')\right\rangle_{\mathcal{E}}\\&\quad=\gamma_a(t)\gamma_a(t')\left\langle\mathcal{O}_a(t)\mathcal{O}_b(t')\right\rangle_{\mathcal{E}}\Theta(t-t')\\&\qquad+\gamma_a(t')\gamma_a(t)\left\langle\mathcal{O}_a(t')\mathcal{O}_a(t)\right\rangle_{\mathcal{E}}\Theta(t'-t),\end{aligned}$$

  where $\mathrm{T_C}$ is the time-ordering for the Keldysh contour. For $\hat{H}_{\mathcal{P}}=0$ we then have $\gamma_a(t)=\gamma_a$. Thus $\gamma_a(t)\gamma_a(t')=1=\gamma_a(t')\gamma_a(t)$ and

$$\begin{aligned}&\left\langle\mathrm{T_C}\,\mathcal{O}_a(t)\gamma_a\gamma_a\mathcal{O}_a(t')\right\rangle_{\mathcal{E}}\\&\quad=\left\langle\mathcal{O}_a(t)\mathcal{O}_b(t')\right\rangle_{\mathcal{E}}\Theta(t-t')+\left\langle\mathcal{O}_a(t')\mathcal{O}_a(t)\right\rangle_{\mathcal{E}}\Theta(t'-t).\end{aligned}$$

  We call the above Green functions the 'Majorana-dressed Green functions', and they are bosonic even if the operators $\mathcal{O}_a$ are fermionic. Moreover, the Majorana-dressed Green functions for the operators $\mathcal{O}_{ab}$ are the same as the undressed ones. Later we denote the Majorana-dressed Green function as $\overline{G}(t,t')$ or $\overline{G}(\omega)$.
- In comparison to the usual Lindblad formalism, for example applying to 1D and 2D topological insulators [24, 25], our formalism is different in two respects. (i) We obtain the reduced density matrix equation (6) directly by utilizing the Clifford algebra of Majorana modes without the need for solving the master equation. (ii) We resum the diagrams in

Gaussian form as opposed to using the Born approximation usually used in the Lindblad formalism, in which the perturbations from the probes are considered only up to second order. Furthermore, we do not assume Markov approximations. As shown later, our results do have some non-Markovian behaviors.

2.4. The environmental influence functional

The second factor of equation (20) is the environmental influence functional for the dynamics of the probe qubits. This is nothing but the product of the real time (bosonic) Green functions of the even parity sectors. Note that the influence functional completely determines the dynamics of the probe, as we set $\hat{H}_{\mathcal{P}} = 0$. From equation (19) we have the following bosonic real time correlation functions appearing in equation (20):

$$\left\langle \tilde{\mathrm{T}}\, \mathcal{H}_m(t)\, \mathrm{T}\, \mathcal{H}_m(t) \right\rangle_{\mathcal{E}}, \tag{21}$$

where $\mathcal{H}_m$ can be either $\cosh \mathbf{O}_M(t)$ or $\sinh \mathbf{O}_M(t)$ with $M = a$ or ab, and we also have

$$\left\langle \tilde{\mathrm{T}}\cosh \mathbf{O}_{ab}(t)\, \mathrm{T}\sinh\mathbf{O}_{ab}(t) \right\rangle_{\mathcal{E}}, \quad \left\langle \tilde{\mathrm{T}}\sinh \mathbf{O}_{ab}(t)\, \mathrm{T}\cosh\mathbf{O}_{ab}(t) \right\rangle_{\mathcal{E}}. \tag{22}$$

In practice, it is difficult to evaluate the real time correlation functions in equation (21) in an exact way. However, in this paper we assume that all the coupling constants, i.e., the B_as and B_{ab}s, are weak, so we first expand these correlation functions up to second order in the coupling constants and then perform the appropriate re-exponentiation [35, 38] in order to approximate the original correlation functions in equation (21), especially their long time behaviors. In this way, the results are expressed in terms of Schwinger–Keldysh Green functions; see appendix A for the detailed definitions.

The aforementioned re-exponentiation procedure is equivalent to resumming the one-particle irreducible diagrams, and should be performed with great care[8] (see appendix B for more detailed discussion) in order to capture the precise long time behavior, at least qualitatively. In the end, we obtain the following results:

$$\left\langle \tilde{\mathrm{T}}\, \cosh \mathbf{O}_M(t)\, \mathrm{T}\, \cosh \mathbf{O}_M(t) \right\rangle_{\mathcal{E}} \approx \frac{1}{2}\left(\mathrm{e}^{2B_M^2 \int^t \mathrm{d}\tau \int^t \mathrm{d}\tau'\, \overline{G}_{M,\mathrm{sym}}(\tau-\tau')} + 1\right), \tag{23}$$

$$\left\langle \tilde{\mathrm{T}}\, \sinh \mathbf{O}_M(t)\, \mathrm{T}\, \sinh \mathbf{O}_M(t) \right\rangle_{\mathcal{E}} \approx \frac{1}{2}\left(\mathrm{e}^{2B_M^2 \int^t \mathrm{d}\tau \int^t \mathrm{d}\tau'\, \overline{G}_{M,\mathrm{sym}}(\tau-\tau')} - 1\right). \tag{24}$$

Here $\overline{G}_{M,\mathrm{sym}}$ is the Majorana-dressed symmetric Green function as defined in equation (A.2). Note that the retarded Green function does not show up in equations (23) and (24).

On the other hand, the correlation functions in equation (22) are related to one-point functions after the expansion up to the second order and re-exponentiating (resumming the tadpole diagrams), e.g.,

$$\left\langle \tilde{\mathrm{T}}\, \cosh \mathbf{O}_{ab}(t)\, \mathrm{T}\, \sinh \mathbf{O}_{ab}(t) \right\rangle_{\mathcal{E}} \approx \mathrm{e}^{B_M \int^t \mathrm{d}\tau\, \langle \mathcal{O}_{ab}(\tau) \rangle_{\mathcal{E}}} - 1, \tag{25}$$

[8] The leading order after expanding $\cosh O_M$ and $\sinh O_M$ is $\mathcal{O}(B_M^2)$, as $\mathcal{O}(B_M)$ has zero expectation value from equation (16). We then re-exponentiate the leading $\mathcal{O}(B_M^2)$ terms without regrouping terms to avoid nontrivial cancellations and express the various propagators in the exponent via equations (A.1)–(A.2).

and thus it vanishes if there is no condensate of $\mathcal{O}_{ab}$. For a nonzero, time-independent, condensate such as the simple mean field result with a superconducting order parameter, equation (25) does not vanish and the reduced density matrix obtained shows oscillating off-diagonal components. Since the bosonic condensate alone will not cause decoherence of the topological qubits, we assume no condensate in this paper, to explore the physics beyond its effect.

2.5. Implications for the dissipationless Majorana modes

From the above results, we see that the time dependence of the reduced density matrix is controlled by the double integral of the symmetric Green functions and the scalar condensates. This is quite different from the case for the usual influence functional for the non-Majorana probe, which in general involves both the retarded and symmetric Green functions [32, 33, 35, 39, 40], i.e., the influence functional takes the form

$$\mathrm{e}^{-g^2\int_{t_i}^{tf}\mathrm{d}\tau\int_{t_i}^{tf}\mathrm{d}\tau'\left[\Delta(\tau)G_{\mathrm{R}}(\tau-\tau')\Sigma(\tau')-\frac{\mathrm{i}}{2}\Delta(\tau)G_{\mathrm{sym}}(\tau-\tau')\Delta(\tau')\right]}, \tag{26}$$

where $\Sigma(\tau)$ and $\Delta(\tau)$ are the center of mass and relative coordinates in the so-called 'ra' (retarded–advanced) basis [32, 37, 42].

In particular, the KMS relation between retarded and symmetric Green functions and their appearance in the Feynman–Vernon influence functional yield the fluctuation-dissipation theorem for the Brownian motion of the probe. More specifically, the Langevin equation derived from the influence functional for the usual Brownian particle takes the form

$$\ddot{\Sigma}+\omega^2\Sigma+g^2\int^t\mathrm{d}\tau\; G_R(t-\tau)\Sigma(\tau)=\xi(t), \tag{27}$$

with

$$\left\langle\xi(t)\xi(t')\right\rangle_{\varepsilon}=g^2G_{\mathrm{sym}}(t-t'). \tag{28}$$

Here, the dissipation term is controlled by the retarded Green function and the fluctuation one is controlled by the symmetric Green function. Thus the KMS relation equation (A.4) yields the fluctuation-dissipation theorem. Furthermore, the kernel for evolving the probe's reduced density matrix is related to the solutions of the Langevin equation equation (27), where the dissipation kernel term $\int^t\mathrm{d}\tau\; G_R(t-\tau)\Sigma(\tau)$ plays an essential role in the reduced dynamics for quantum decoherence; for example see [32, 35, 36, 40].

Our method is different from the Feynman–Vernon one, so our 'influence functional' may not be exactly the same as the Feynman–Vernon one. However, due to the physical similarity between these two, it is tempting to say that the absence of the retarded Green function in the influence functional for the Majorana mode implies that its dynamics is dissipationless.

The feature of the Majorana mode of being dissipationless is expected, as its transport is related to anomalous transport [50], which has been shown to be dissipationless hydrodynamically, i.e., there is no generation of entropy [51]. Intuitively, if the environment is not topologically ordered, and so cannot produce a dangling Majorana mode to combine with the endpoint one to form an electron, then the endpoint Majorana mode is robust. However, there is still a possibility that the environment's electron deconfines into a pair of Majorana modes, one of them combining with the endpoint Majorana mode to turn into an endpoint electron, and the other leaking into the environment. This is in fact captured by the interaction

Hamiltonian $\hat{V}$ of equation (3), which implies that the endpoint Majorana mode can turn into an electron mode.

For the whole system the interaction Hamiltonian still preserves the Majorana mode number; we can think that the endpoint Majorana mode just moves into the bulk. However, from the point of view of the open system the endpoint Majorana mode just dissipates away or thermalizes. Despite that, our resultant 'influence functional' with the absence of a retarded Green function suggests that the feature of the Majorana modes of being dissipationless may still be preserved to some extent even under the effect of the interaction Hamiltonian. To pin down more specifically the feature of being dissipationless for the Majorana modes and understand the fluctuation-dissipation theorem in the sense of Langevin, one may need to derive the Feynman–Vernon influence functional. We will not consider this issue further in this work. Instead, it is interesting to ask whether such a possible feature of being dissipationless also implies robustness against decoherence or not.

Recall the fact that the Fourier transform of the symmetric Green function encodes the spectral density of the corresponding channel for fluctuation and dissipation. However, the dissipation ability of the effective carriers for decoherence is given by $\int^t \mathrm{d}\tau \int^t \mathrm{d}\tau'\, \overline{G}_{M,\mathrm{sym}}(\tau - \tau')$, as suggested in equations (23) and (24). Thus, there is a possibility that the effective carriers are not so efficient at carrying away the quantum information of the topological qubits as the spectral density implies. We see that this is indeed the case in the next section.

3. Decoherence patterns of topological qubits

Now we are ready to apply the above formal results in studying the patterns of decoherence of the topological qubits in various environments. As the influence functional due to the environment (taking the form of $\int^t \mathrm{d}\tau \int^t \mathrm{d}\tau'\, \overline{G}_{M,\mathrm{sym}}(\tau - \tau')$ in our case) affects the decoherence pattern, one should specify the dynamics of the environment if one wishes to obtain concrete results. For the fermionic environment we consider the setup of a quantum wire [17, 18] tunnel coupled to superconducting wires as shown in figure 1. We take the helical Luttinger wire [48], which can be realized as the edge state of some two-dimensional topological insulator [46], as a special example, but the generalization to other kinds of Luttinger liquids [47] is straightforward. For the bosonic environment we take the ring structure [19], as shown in figure 2, with external magnetic flux Φ controlling different frequency modes of bosonic couplings. In general the Majorana modes could also be realized in a cold atom setup [20] and the local bosonic couplings can also be achieved in cold atom systems with tunable interacting bosonic environments. We assume that the bosonic environments are also described by conformally invariant theory and take the special case of AdS_5 space holographic theory.

3.1. The environmental influence function of helical Luttinger liquids and its CFT generalizations

The typical environments composed of 1D electrons are either Fermi or Luttinger liquids. For the helical Luttinger liquid wire case the Majorana-dressed symmetric Green function with election chemical potential μ takes the following form (for more details, see appendix C.1):

$$\overline{G}_{a,\mathrm{sym}}(\omega) = c_1(\kappa)\,|\omega-\mu|^{2\kappa-1}\,\mathrm{e}^{-\frac{\omega^2}{\Gamma_0^2}} \quad (\kappa \geqslant 1/2), \tag{29}$$

where $\kappa \equiv \left(K+\frac{1}{K}\right)\Big/4$, with K denoting the Luttinger parameter, is related to the conformal dimension of the operator $\mathcal{O}_a$ and is used to characterize the Luttinger liquid, e.g., $\kappa = 1/2$ for Fermi liquid. A rough estimate of the Luttinger parameter K is given by $K^2 \sim (1+\frac{U}{2\epsilon_\mathrm{F}})$, where ϵ_F is the Fermi energy and $U \sim \frac{e^2}{\epsilon a_0}$ (ϵ being the dielectric constant and a_0 being the lattice length) is the characteristic Coulomb energy of the wire [47]. Thus the value of κ can be tuned by changing the effective repulsive/attractive short range interactions in the wire. $c_1(\kappa)$ is some function of κ and its exact form is given in appendix C.1. We have introduced in equation (29) a windowed function $\mathrm{e}^{-\omega^2/\Gamma_0^2}$ to impose a cutoff on the high frequency modes, but the main results that we mention below do not depend on this choice of cutoff.

Similarly, for the bosonic operators $\mathcal{O}_{ab}$ of conformal dimension Δ, the associated Majorana-dressed symmetric Green function is (for more details, see appendix C.2)

$$\overline{G}_{ab,\mathrm{sym}}(\omega) = c_2(\Delta)\,|\omega|^{2\Delta-4}\,\mathrm{e}^{-\frac{\omega^2}{\Gamma_0^2}} \quad (\Delta \geqslant 2), \tag{30}$$

where $c_2(\Delta)$ is some analytic function of Δ and its explicit form is given in appendix C.2.

For equations (29) and (30) we carry out the double time integration, and the results are

$$\int^t \mathrm{d}\tau \int^t \mathrm{d}\tau'\, \overline{G}_{a,\mathrm{sym}}(\tau-\tau') = \frac{c_1(\kappa)}{\Gamma(2\kappa)} I_{2\kappa-1}\left(t;\,\mu,\,\Gamma_0\right) \tag{31}$$

for $\mathcal{O}_a$, and

$$\int^t \mathrm{d}\tau \int^t \mathrm{d}\tau'\, \overline{G}_{ab,\mathrm{sym}}(\tau-\tau') = c_2(\Delta) I_{2\Delta-4}\left(t;\,0,\,\Gamma_0\right) \tag{32}$$

for $\mathcal{O}_{ab}$, with

$$I_Q\left(t;\,\mu,\,\Gamma_0\right) := \int_0^\infty \left(|\omega+\mu|^Q + |\omega-\mu|^Q\right) \frac{2-2\cos\omega t}{\omega^2}\,\mathrm{e}^{-\frac{\omega^2}{\Gamma_0^2}}\,\mathrm{d}\omega. \tag{33}$$

For the $\mu = 0$ case, the integral in equation (33) is worked out as (for $Q \geqslant 0$)

$$\begin{aligned} I_Q\left(t;\,0,\,\Gamma_0\right) &= 4\int_0^\infty |\omega|^Q \frac{1-\cos\omega t}{\omega^2}\mathrm{e}^{-\frac{\omega^2}{\Gamma_0^2}} \\ &= \begin{cases} 2\Gamma_0^{Q-1}\Gamma\left(\dfrac{Q-1}{2}\right)\left(1 - {}_1F_1\left(\dfrac{Q-1}{2};\,\dfrac{1}{2};\,-\dfrac{t^2\Gamma_0^2}{4}\right)\right) \\ \qquad \text{for} \quad Q \geqslant 0 \quad \text{but} \quad Q \neq 1; \\ \dfrac{1}{2}t^2\Gamma_0^2\ {}_2F_2\left(\{1,\,1\};\,\left\{\dfrac{3}{2},\,2\right\};\,-\dfrac{t^2\Gamma_0^2}{4}\right) \\ \qquad \text{for} \quad Q = 1. \end{cases} \end{aligned} \tag{34}$$

Here ${}_pF_q(\{a_1,\,\ldots,\,a_p\};\,\{b_1,\,\ldots,\,b_q\};\,z) = \sum_{k=0}^\infty \frac{(a_1)_k \cdots (a_p)_k}{(b_1)_k \cdots (b_q)_k}\frac{z^k}{k!}$ is the generalized hypergeometric function, and $\Gamma(z)$ is the Gamma function.

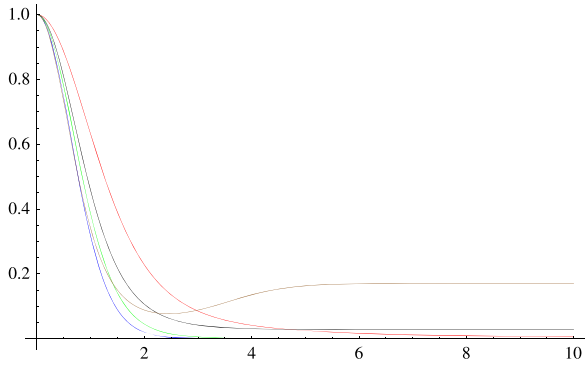

Figure 3. $e^{-I_Q(t;\mu=0,\Gamma_0=1)}$ versus t for $Q = 0.5$ (blue), 0.9 (green), 1 (red), 2 (black) and 4 (brown). This factor controls the time dependence of the influence functional. We can see that there is a critical value at $Q = 1$ beyond which this factor will have a drop–dip–flat pattern and will not decay to zero.

First, we see that the behavior of equation (34) at $t \approx 0$ is universal, i.e., $I_Q \propto t^2$ independently of Q. Using this, it is straightforward to show the following universal tsunami behavior of the entanglement growth as discussed in [40, 41]:

$$S_2 = -\ln \mathrm{Tr}\, \rho_r^2 \propto t^2 \qquad \text{for} \quad t \approx 0. \tag{35}$$

Note that S_2 is the second-order Renyi entropy, which characterizes the quantum entanglement between the probe and the environment. The above t^2 growth is more rapid than the t growth expected from the causality argument, and is thus called tsunami behavior. However, this tsunami behavior will soon be taken over by t growth once the spreading scale is above the size of the probe.

On the other hand, the late time behavior of equation (34) has an interesting turning point at $Q = 1$, i.e., $\kappa = 1$ or $\Delta = 2.5$. For $Q \leqslant 1$ (Ohmic and sub-Ohmic environments) the magnitude of the hypergeometric function in equation (34) increases monotonically with increasing time t. However, for $Q > 1$ (super-Ohmic environments) it decreases to zero at large time, so $I_Q(t; 0, \Gamma_0) \to 2\Gamma_0^{Q-1}\Gamma\left(\frac{Q-1}{2}\right)$ as $t \to \infty$. See figure 3 for $e^{-I(t;\mu=0,\Gamma_0)}$ for this change of behavior on varying Q. This qualitative change of the time dependence has two implications:

- There should be a metal–insulator-like quantum phase transition, similarly to the case for electric transport [48], obtained by tuning Q for the probe state, due to the back-reaction of integrating out the environment. For $Q \leqslant 1$, the number of effective carriers quantified by equation (34) is sufficient for the probe state to be delocalized and dissipative. In contrast, for $Q > 1$, the effective carriers are insufficient, so the state is localized and nondissipative.
- As the probe carries both energy and quantum information, the delocalization of the probe state also implies leakage of the quantum information into the environment. This finally leads to complete decoherence. Otherwise, the quantum information is confined around the localized probe state and only partially leaks into the environment. For such a case, one may further purify the probe state to recover and maintain the quantum information carried by the probe. Although our interpretation of the incomplete

decoherence for our setup is quite different from the usual one from non-Markovian dynamics, which is mainly as due to due to the gap-like structures of the environmental spectral densities [45], we do see similar information backflow for $Q > 1$ cases (as seen from the drop–dip–flat patterns of the purity shown below), characterizing the non-Markovian dynamics.

The above picture of a quantum phase transition might be understood via the renormalization group (RG) argument for the coupling constant B_M. Note that the fermionic environment that we choose in this paper is the helical Luttinger liquids, which can be realized as interacting edge states of two-dimensional topological insulators [46, 48]. For this kind of fermionic environment, the scaling dimension from zeroth-order renormalization group analysis [48, 49] for the interaction $\hat{V}$ is κ. This yields the renormalized coupling B_a in the linear response regime as

$$\frac{\mathrm{d}B_a}{\mathrm{d}\ln(\Gamma_0)} = (1 - \kappa)B_a, \tag{36}$$

with $\Gamma_0 \simeq \hbar v/a_0$ as the UV cutoff for the linear spectrum of the edge state. For the electric transport discussed in [48], $\kappa = 1$ indicates the critical interaction strength for metallic–insulating behavior. That is, following equation (36) we see that for $1 \geqslant \kappa \geqslant 1/2$ the coupling B_a increases as the cutoff decreases, while for $\kappa > 1$ the coupling B_a decreases with decreasing cutoff, indicating insulating behavior for the charge transport.

3.2. Pointer states, purity and concurrence

Though the time dependence of equation (34) provides a very suggestive picture for the change of the decoherence pattern on tuning Q, one should still study the detailed form of the final reduced density matrix, from which we derive some quantities for characterizing the decoherence patterns.

There are many ways to characterize the quantum decoherence. If the probe state is in the basis of pointer states [52], then we can characterize the decoherence by observing the time evolution of the off-diagonal elements of the reduced density matrix. If all of the off-diagonal elements vanish in the long run, then the final reduced density matrix is in a pointer state. In this case, the probe state decoheres completely. Among the pointer states, a special one is the Gibbs state with all of the diagonal elements equal. For such a case, we can furthermore claim that the probe state has been thermalized (at zero temperature).

However, if the final state does not reduce to a pointer state, then we shall find some quantity to characterize the quantumness of the probe state. In this work we choose the purity

$$\mathcal{P}^{\mathrm{b,f}} := \mathrm{Tr}\,\rho^2, \tag{37}$$

where the superscripts b and f refer to bosonic and fermionic environments. The purity is related to the second-order Renyi entropy by $S_2 := -\ln \mathcal{P}^{\mathrm{b,f}}$.

Note that without knowing whether all of the off-diagonal elements of the reduced density matrix diminish or not, one cannot tell from the purity alone whether the qubits decohere completely except for the Gibbs state. The purity of the N-qubit state reaches its minimal value $\frac{1}{N}$ for the Gibbs state. Thus, a thermalized state is definitely a classical state.

For multi-qubit cases, one can also characterize the decoherence through the time evolution of the quantum entanglement among the qubits. For the two-qubit case this is faithfully characterized by the concurrence [53]:

$$C(\rho) := \max\left(0, \lambda_1 - \lambda_2 - \lambda_3 - \lambda_4\right), \tag{38}$$

where $\lambda_1, \cdots, \lambda_4$ are the square roots of the eigenvalues, in decreasing order, of $\rho\tilde{\rho}$ with $\tilde{\rho} := (\sigma_y \otimes \sigma_y)\rho^*(\sigma_y \otimes \sigma_y)$, for σ_y the Pauli matrix. If the final probe state is a pointer state, i.e., completely decohered, then $C = 0$ at large time as the quantum entanglement is an essential property only for a quantum state. But the inverse is not true as the quantum state may not be entangled.

3.3. Cases with single topological qubits

In the first case, we consider only two Majorana modes γ_1 and γ_2 living on two ends of a quantum wire, which couple locally to the surrounding electrons via the channels $\mathcal{O}_E$ appearing in the interaction equation (3). Before one turns on the interaction equation (3), these two Majorana modes form a topological (nonlocal) qubit with state $|0\rangle$ and $|1\rangle$ connected by

$$\frac{1}{2}\left(\gamma_1 - \mathrm{i}\gamma_2\right)|0\rangle = |1\rangle, \qquad \frac{1}{2}\left(\gamma_1 + \mathrm{i}\gamma_2\right)|1\rangle = |0\rangle. \tag{39}$$

We can choose the following representation for $\gamma_{1,2}$:

$$\gamma_1 = \sigma_1, \qquad \gamma_2 = \sigma_2, \qquad \mathrm{i}\gamma_1\gamma_2 = \sigma_3 \tag{40}$$

where the σ_as are the Pauli matrices, thus satisfying $\gamma_a^\dagger = \gamma_a$ and $\{\gamma_a, \gamma_b\} = 2\delta_{ab}$. Note that $\mathrm{i}\gamma_1\gamma_2$ defines a parity operator for the states of the topological qubit, i.e.,

$$\mathrm{i}\gamma_1\gamma_2\,|0\rangle = |0\rangle, \qquad \mathrm{i}\gamma_1\gamma_2\,|1\rangle = -|1\rangle. \tag{41}$$

Obviously, the interactions $\gamma_1\mathcal{O}_1$ and $\gamma_2\mathcal{O}_2$ flip the parity of the topological qubit but $\gamma_1\gamma_2\mathcal{O}_{12}$ does not.

In this representation, the generic initial state of the probe can be cast as a Hermitian matrix with positive eigenvalues:

$$\rho_{\mathcal{P}}(t=0) = \begin{pmatrix} a_{00} & a_{01} \\ a_{01} & a_{11} \end{pmatrix}, \tag{42}$$

with $a_{00} + a_{11} = 1$.

Here we consider either (i) a fermionic environmental channel with the evolution operator $U(t) = \mathrm{T}\,\mathrm{e}^{-\mathrm{i}\gamma_1\mathbf{O}_1(t)}\mathrm{e}^{-\mathrm{i}\gamma_2\mathbf{O}_2(t)}$ or (ii) a bosonic environmental channel with $U = \mathrm{e}^{-\mathrm{i}\gamma_1\gamma_2\mathbf{O}_{12}(t)}$. Using equation (20), the explicit form of the reduced density matrix at time t is

$$\rho_{\mathrm{r}}^{\mathrm{f}}(t) = \frac{1}{N^{\mathrm{f}}(t)}\begin{pmatrix} a_{00}\left(C_1C_2 + S_1S_2\right) - a_{11}\left(C_2S_1 + C_1S_2\right) & a_{01}\left(C_1C_2 - S_1S_2\right) - a_{10}\left(C_2S_1 - C_1S_2\right) \\ a_{10}\left(C_1C_2 - S_1S_2\right) - a_{01}\left(C_2S_1 - C_1S_2\right) & a_{11}\left(C_1C_2 + S_1S_2\right) - a_{00}\left(C_2S_1 + C_1S_2\right) \end{pmatrix} \tag{43}$$

for the fermionic channel, and

$$\rho_{\rm r}^{\rm b}(t)=\frac{1}{N^{\rm b}(t)}\begin{pmatrix} a_{00}\big(C_{12}-S_{12}\big) & a_{01}\big(C_{12}+S_{12}\big)\\ a_{10}\big(C_{12}+S_{12}\big) & a_{11}\big(C_{12}-S_{12}\big)\end{pmatrix} \tag{44}$$

for the bosonic channel. In the above, the normalization factor $N^{\rm f,b}(t)=\mathrm{Tr}\,\rho_{\rm r}^{\rm f,\,b}(t)$, and

$$C_M\equiv\left\langle\tilde{\mathrm{T}}\cosh\mathbf{O}_M(t)\,\mathrm{T}\cosh\mathbf{O}_M(t)\right\rangle_{\mathcal{E}}, \tag{45}$$

$$S_M\equiv\left\langle\tilde{\mathrm{T}}\sinh\mathbf{O}_M(t)\,\mathrm{T}\sinh\mathbf{O}_M(t)\right\rangle_{\mathcal{E}} \tag{46}$$

for M equal to either a or ab. Their relations with the Majorana-dressed symmetric Green functions are given in equations (23) and (24).

Note that there is a key difference between equations (43) and (44). In equation (43) the states with different parities, i.e., $|0\rangle\langle 0|$ and $|1\rangle\langle 1|$, or $|0\rangle\langle 1|$ and $|1\rangle\langle 0|$, mix as time evolves, but this does not happen in equation (44). This is for the reason stated below equation (40), i.e., the fermionic environments flip the parity of the topological qubit but the bosonic ones do not.

We further simplify the above reduced density matrices by assuming that all of the Majorana modes couple to the same environments with the same coupling strengths. Under this condition we can omit the subscripts M of $\overline{G}_{M,\rm sym}$ and B_M as they are all the same. The reduced density matrix is then simplified to

$$\rho_{\rm r}^{\rm f}(t)=\frac{1}{2}\begin{pmatrix} 1+\big(2a_{00}-1\big)\alpha^2(t) & 2a_{01}\alpha(t)\\ 2a_{10}\alpha(t) & 1+\big(2a_{11}-1\big)\alpha^2(t)\end{pmatrix} \tag{47}$$

and

$$\rho_{\rm r}^{\rm b}(t)=\begin{pmatrix} a_{00} & a_{01}\alpha(t)\\ a_{10}\alpha(t) & a_{11}\end{pmatrix} \tag{48}$$

where the influence functional

$$\alpha(t)=\mathrm{e}^{2B^2\int^t\mathrm{d}\tau\int^t\mathrm{d}\tau'\,\overline{G}_{\rm sym}(\tau-\tau')}=\mathrm{e}^{-2B^2\left|\alpha_{1,2}\right|I_Q(t;\mu=0,\Gamma_0)}, \tag{49}$$

where the $\alpha_{1,2}$s are the time-independent overall coefficients in front of the Majorana-dressed symmetric Green functions given in equations (C4) and (C6*b*), respectively. Note that these coefficients are negative.

The typical behaviors of $\alpha(t)$ for varying Q can be inferred from figure 3. The factor $2B^2|\alpha_{1,2}|$ in equation (49) will only affect the behaviors in figure 3 quantitatively, and not qualitatively. Thus, there is a critical point at $Q=1$ for $\alpha(t)$. For $Q\leqslant 1$ (Ohmic and sub-Ohmic), $\alpha(t)$ vanishes at large t, so the state of the topological qubit reduces to a pointer state in both the fermionic and the bosonic environments. This implies that the topological qubits decohere completely. However, there is a key difference between fermionic and bosonic cases: the pointer state in the (parity-flipping) fermionic environments is the Gibbs state, but this is not the case in the (parity-conserving) bosonic ones. The reduction to the Gibbs state means thermalization (in the sense of the microcanonical ensemble). The thermalization is due to the mixing of the parity odd and even states caused by the parity-violating interactions. In contrast, there is no mixing in the bosonic case, so the diagonal elements of equation (48)

remain constant, not going to 1/2 as the off-diagonal elements diminish. We can then conclude that in the sub-Ohmic environments, although the parity conservation cannot prevent a topological qubit from exhibiting complete decoherence, it can prevent it from exhibiting complete thermalization[9]. Note that the term 'thermalization' here is used in the context of the microcanonical ensemble for our zero-temperature setup or in the context of closed system (probe plus environment) thermalization. For considering the topological qubits in contact with the thermal environment, a new observable characterizing the topological nature of the Majorana modes should be constructed [26].

For both kinds of environments at $Q > 1$ (super-Ohmic), $\alpha(t)$ reduces to a nonzero constant at late time, so the off-diagonal elements of the reduced density matrices do not vanish. This implies that the probe state cannot completely decohere, and the incomplete decoherence can be quantified by the purity equation (37).

In the fermionic cases, the parameter κ characterizes the interaction strengths of the Luttinger/Fermi liquid. The larger κ, the stronger the interaction/correlation shown by the Luttinger liquid nanowire. Our above results suggest that the strongly correlated environments help to preserve the quantum information of the probe even if the probe–environment coupling is weak. This can be understood as follows: the weakly coupled probe–environment contact spot becomes a peculiar point, contrasting with the strongly coupled neighbors, so the quantum information stays around this particular place.

We consider in section 3.4 the cases of nonuniform environments. We still keep the coupling strengths $B_M = B$ uniform in order to focus on the effect of varying the environmental spectral functions $\overline{G}_{M,\mathrm{sym}}$ with M. The tuning $B_M = B$ is achievable in the experiments, by controlling the gate voltages of the various tunneling junctions.

3.4. Nonuniform environments

As the topological qubit is nonlocal, it is interesting to consider a peculiar case which cannot happen for the usual local qubit—that is, the nonuniform environment. In this case, the two Majorana modes can couple to environments of different κs, say, κ_1 and κ_2. Given the initial state equation (42), the reduced density matrix $\rho_{\mathrm{r}}^{\mathrm{f}}(t)$ with two different κs takes the form

$$\begin{pmatrix} \frac{1}{2} + \alpha_1(t)\alpha_2(t)\left(a_{00} - \frac{1}{2}\right) & \alpha_2(t)\,\mathrm{Re}\,a_{01} + \mathrm{i}\alpha_1(t)\,\mathrm{Im}\,a_{01} \\ \alpha_2(t)\,\mathrm{Re}\,a_{01} - \mathrm{i}\alpha_1(t)\,\mathrm{Im}\,a_{01} & \frac{1}{2} - \left(a_{00} - \frac{1}{2}\right)\alpha_2(t)\alpha_1(t) \end{pmatrix}, \tag{50}$$

[9] Another way to see this is through the counting of Majorana fermions involved in the coupling terms. For odd number of Majorana fermions (generic fermionic environments) the even and odd fermion initial states could mix through this interaction, leading to thermalized states, as expected, while for even number of Majorana fermions (bosonic environments) the even/odd fermion states could only mix with even/odd states. Thus the bosonic environments bring in this additional symmetry which prevents the thermalization in the sub-Ohmic environments. Parity-preserving coupling, which is the same as Majorana fermion number counting for a single qubit but different for the two-qubit case, imposes an even stronger constraint such that the even/odd states do not mix with other even/odd states, keeping the diagonal components intact at the long time limit. For super-Ohmic environments, both fermionic and bosonic environments do not decohere and thus they do not reach pointer states.

from which one can obtain the purity as follows:

$$\mathcal{P}^{\mathrm{f}}(t) = \frac{1}{2} + 2\left[\mathrm{Im}\, a_{01}\right]^2 \alpha_1^2(t)\left(1 - \alpha_2^2(t)\right) + 2\left[\mathrm{Re}\, a_{01}\right]^2 \alpha_2^2(t) \tag{51}$$

where

$$\alpha_1(t) = \mathrm{e}^{2B^2 \int^t \mathrm{d}\tau \int^t \mathrm{d}\tau' \, \overline{G}_{1,\mathrm{sym}}(\tau-\tau')}, \tag{52}$$

$$\alpha_2(t) = \mathrm{e}^{2B^2 \int^t \mathrm{d}\tau \int^t \mathrm{d}\tau' \, \overline{G}_{2,\mathrm{sym}}(\tau-\tau')}, \tag{53}$$

with $\overline{G}_{1,\mathrm{sym}}$ and $\overline{G}_{2,\mathrm{sym}}$ corresponding to the Majorana-dressed symmetric Green functions of κ_1 and κ_2, respectively. In arriving at equation (51) we have used the fact that $\rho_{\mathcal{P}}(t=0)$ is Hermitian, so $a_{10} = a_{01}^*$. As $\alpha_{1,2}^2(t)$ are always smaller than 1, the expression equation (51) implies that $\mathcal{P}^{\mathrm{f}}(t) \geqslant 1/2$. Note that $\mathcal{P}^{\mathrm{f}} = 1/2$ corresponds to the Gibbs state.

From equation (50), we see that if $\alpha_{1,2}$ have the same late time behaviors, then the decoherence patterns are qualitatively similar to the cases with uniform environments. Otherwise we find new decoherence patterns. More specifically, for uniform environments the final state purity depends both on Im a_{01} and on Re a_{01}. On the other hand, for the nonuniform environment with different late time behaviors, equation (50) shows bias, that is, the first channel favors the initial state with nonzero Im a_{01} being robust against complete decoherence, and the second channel favors that with nonvanishing Re a_{01}. This suggests that the information of the real part and that of the imaginary part of off-diagonal reduced density matrix element a_{01} are carried by different endpoints of Majorana modes. Thus, the decoherence pattern not only depends on the environments but also on the initial states. Note that this kind of nonuniformity of the environments is a peculiar feature of the topological qubit composed of Majorana modes.

We would like to illustrate the implication of the above results more here. In the context of a closed system, all of the single-qubit pure states are connected by unitary transformations and thus are equivalent. For local qubits these unitary transformations can be performed locally, but for the topological qubits nonlocal unitary operations are needed. However, once the qubits are put in contact with the environments, the unitarity is lost as time evolves and the naive equivalence of all of the pure states no longer holds. The loss of unitarity implies that the 'democracy' of pure states representing quantum information is broken, and some states are more robust against decoherence than others. From our above discussions, we see that the nonuniformity of the environments further enhances the inequality among the pure states. The state space of a single qubit is represented by a Bloch sphere, and the breaking of state 'democracy' implies spontaneous breaking of the isometry of the Bloch sphere. The nonuniformity of the environments breaks the isometry even more.

As shown, the decoherence pattern of a single topological qubit can be read out directly from the time dependence of the reduced density matrix. This is not the case for the generic initial states of two topological qubits (formed from four Majorana fermions) due to the complexity of the analytical formula. We numerically plot the purity and concurrence for characterizing the decoherence patterns for those cases in section 3.5.

3.5. Cases with two topological qubits

Now we consider the cases with two topological qubits made up of four Majorana modes. The Hilbert spaces of two qubits are spanned by $\{|00\rangle, |01\rangle, |10\rangle, |11\rangle\}$, which are connected by

$$d_1^\dagger |00\rangle \equiv \frac{1}{2}\left(\gamma_1 - \mathrm{i}\gamma_2\right)|00\rangle = |10\rangle, \tag{54a}$$

$$d_2^\dagger |00\rangle \equiv \frac{1}{2}\left(\gamma_3 - \mathrm{i}\gamma_4\right)|00\rangle = |01\rangle, \tag{54b}$$

$$d_1^\dagger d_2^\dagger |00\rangle = |11\rangle. \tag{54c}$$

Generalizing the case of the single topological qubit, here we can define two commuting parity operators for the states of two topological qubits, i.e.,

$$\mathrm{i}\gamma_1\gamma_2 |jk\rangle = (-1)^j |jk\rangle, \quad \mathrm{i}\gamma_3\gamma_4 |jk\rangle = (-1)^k |jk\rangle, \tag{55}$$

with $j, k = 0,1$. Note that other two-gamma operators such as $\mathrm{i}\gamma_1\gamma_3$ are not parity operators. From these facts, we know that the interactions $\gamma_1\gamma_2\mathcal{O}_{12}$ and $\gamma_3\gamma_4\mathcal{O}_{34}$ preserve the parity of the topological qubit but the other interactions do not. Furthermore, if we consider also interactions involving four Majorana modes, i.e., $\gamma_1\gamma_2\gamma_3\gamma_4\mathcal{O}_{1234}$, we may also introduce another parity operator, $\Gamma^{(4)} := -\gamma_1\gamma_2\gamma_3\gamma_4$, which also commutes with the previous two parity operators, i.e.,

$$\Gamma^{(4)} |jk\rangle = (-1)^{j+k} |jk\rangle. \tag{56}$$

Thus, $|00\rangle$ and $|11\rangle$ are $\Gamma^{(4)}$-parity even states and $|01\rangle$ and $|10\rangle$ are odd states. This echoes the choice of using $|00\rangle$ and $|11\rangle$ as a single topological qubit [21–23] if we deemed the effective p-wave superconductor in the Kitaev chain to be a kind of external bosonic environment for the Majorana endpoints.

As the Majorana fermions obey the Clifford algebra: $\{\gamma_i, \gamma_j\} = 2\delta_{ij}$, we can then choose the following representation:

$$\begin{aligned} \gamma_1 &= \sigma_1 \otimes \sigma_0, \quad \gamma_2 = \sigma_2 \otimes \sigma_0, \\ \gamma_3 &= \sigma_3 \otimes \sigma_1, \quad \gamma_4 = \sigma_3 \otimes \sigma_2. \end{aligned} \tag{57}$$

The generic initial density matrix for the probe is given by a 4×4 Hermitian matrix with positive eigenvalues. For general initial state, obtaining the explicit form of $\rho_t(t)$ following from equation (20) is very tedious. Since we are considering quantum decoherence, we take the initial state as a pure state with the following form:

$$\left|(e_1, e_2, e_3, e_4)\right\rangle = e_1\left|00\right\rangle + e_2\left|01\right\rangle + e_3\left|10\right\rangle + e_4\left|11\right\rangle, \tag{58}$$

with $|e_1|^2 + |e_2|^2 + |e_3|^2 + |e_4|^2 = 1$.

In the following we assume that the fermionic channel takes the form $\gamma_i\mathcal{O}_i$ and that the bosonic channel takes the forms $\gamma_1\gamma_2\mathcal{O}_{12}$ and $\gamma_3\gamma_4\mathcal{O}_{34}$ which are parity-preserving. All of the numerical plots shown below are for these interactions.

On the other hand, the effect of bosonic parity-violating couplings such as $\gamma_1\gamma_3\mathcal{O}_{13}$ and $\gamma_2\gamma_4\mathcal{O}_{24}$ is briefly discussed here. We wonder whether these interactions will mix the different parity sectors and lead to thermalization in the (uniform) sub-Ohmic environments as for the fermionic cases. The answer is that they will not, as seen from the final state density matrix for the given initial state equation (58), i.e.,

$$\rho_{\rm r}^{\rm b}(\infty)=\begin{pmatrix}\frac{|e_1|^2+|e_4|^2}{2} & 0 & 0 & 0\\ 0 & \frac{|e_2|^2+|e_3|^2}{2} & 0 & 0\\ 0 & 0 & \frac{|e_2|^2+|e_3|^2}{2} & 0\\ 0 & 0 & 0 & \frac{|e_1|^2+|e_4|^2}{2}\end{pmatrix}. \tag{59}$$

equation (59) shows that parity-violating bosonic couplings mix even parity states with other even parity states but not odd ones (and similarly, odd parity states can only mix with other odd parity states)[9].

Now we will start our numerical case studies. For illustration, we first consider a special case with the initial state of the topological qubits being $|(e_1, 0, 0, e_4)\rangle$, which corresponds to the initial state density matrix

$$\rho_{\mathcal{P}}(t=0)=\begin{pmatrix}|e_1|^2 & 0 & 0 & e_1e_4^*\\ 0 & 0 & 0 & 0\\ 0 & 0 & 0 & 0\\ e_1^*e_4 & 0 & 0 & |e_4|^2\end{pmatrix}. \tag{60}$$

Furthermore, we assume that the fermionic channel takes the form $\gamma_i\mathcal{O}_i$ and that the bosonic channel takes the forms $\gamma_1\gamma_2\mathcal{O}_{12}$ and $\gamma_3\gamma_4\mathcal{O}_{34}$. For such cases, the reduced density matrices are given in equation (E1) for the fermionic channel and in equation (E2) for the bosonic channel. If we consider the uniform environment as in the single-qubit case, then we can further simplify the reduced density matrix. The results are as follows:

$$\rho_{\rm r}^{\rm f}(t)=\frac{1}{4}\begin{pmatrix}A_{11} & 0 & 0 & A_{14}\\ 0 & A_{22} & 0 & 0\\ 0 & 0 & A_{33} & 0\\ A_{41} & 0 & 0 & A_{44}\end{pmatrix}, \tag{61}$$

with $A_{11}=1+\alpha(t)^4+2(2|e_1|^2-1)\alpha(t)^2$, $A_{22}=A_{33}=1-\alpha(t)^2$, $A_{44}=1+\alpha(t)^4+2(2|e_4|^2-1)\alpha(t)^2$ and $A_{14}=A_{41}^*=4e_1e_4^*\alpha(t)^2$, and

$$\rho_{\rm r}^{\rm b}(t)=\begin{pmatrix}|e_1|^2 & 0 & 0 & e_1e_4^*\alpha(t)^2\\ 0 & 0 & 0 & 0\\ 0 & 0 & 0 & 0\\ e_1^*e_4\alpha(t)^2 & 0 & 0 & |e_4|^2\end{pmatrix}. \tag{62}$$

Like for the single-qubit case discussed in section 3.3, for $Q>1$ the topological qubits cannot decohere completely for both fermionic and bosonic environments. For $Q\leqslant 1$, $\rho_{\rm r}^{\rm f}(t)$ reduces to the Gibbs state and $\rho_{\rm r}^{\rm b}(t)$ reduces to a special pointer state at large time, indicating that the topological qubits decohere completely, but only thermalize in the fermionic environments.

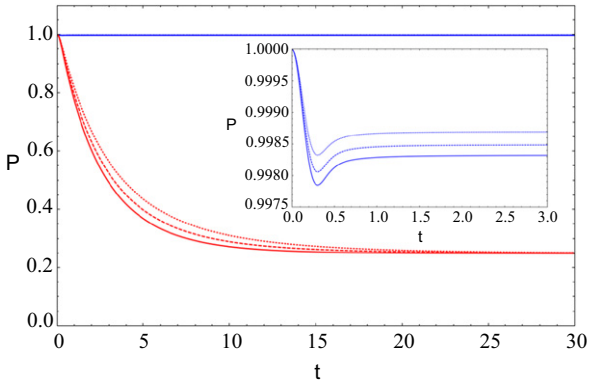

Figure 4. Purity versus t for $\kappa = 0.5$ (red) and $\kappa = 2$ (blue) with initial states $|(e_1, e_2, e_3, e_4)\rangle = |(1, 0, 0, 1)\rangle$ (solid), $|(2, 1, 0, 2)\rangle$ (dashed), and $|(1, 1, 0, 1)\rangle$ (dotted). The inset shows a magnification of the early time region for $\kappa = 2$ cases.

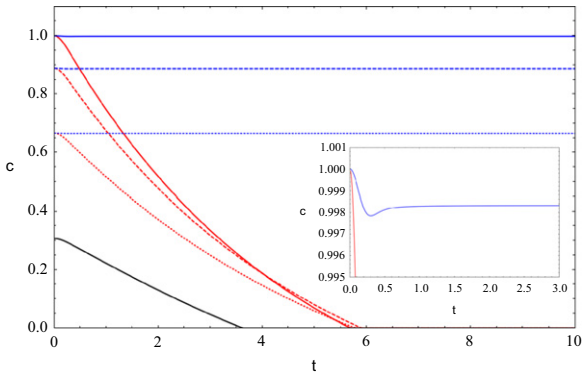

Figure 5. Concurrence versus t for the states and environments specified in figure 4. The inset shows the solid lines enlarged at short time. Here we add a black solid line representing the concurrence pattern of the initial state $|(e_1, e_2, e_3, e_4)\rangle = |(2, 2, 1, 2)\rangle$ in the $\kappa = 0.5$ environment to show that its concurrence does not diminish with the other red lines at the same time.

Thus with bosonic (parity-preserving and parity-violating) couplings the topological qubits decohere, but in general thermalized states are not reached in the sub-Ohmic environments, as shown later in figures 6 and 10, in which the purity never reaches 1/4 even for sub-Ohmic lines.

Now, we consider the decoherence patterns for various initial states $|(e_1, e_2, e_3, e_4)\rangle$. As obtaining the explicit form of the reduced density matrix is quite tedious and not very illuminating, we directly present numerical plots. We first consider the uniform environment and plot the decoherence patterns for various initial states $|(e_1, e_2, e_3, e_4)\rangle$. In each plot we compare the decoherence patterns (either purity or concurrence ones) for the $Q \leqslant 1$ and $Q > 1$ cases with the same given initial states. The results are shown in figures 4–7. We then consider some cases for the nonuniform environment, and the results are plotted in figures 8–11.

Moreover, in all the following plots we set $B = 0.1$, the cutoff $\Gamma_0 = 10$, the parameters a_0/v in equation (C4) and ϵ in equation (C6) to $1/\Gamma_0$, and the parameter N_{sc} in equation (C6) to 1. The unit of the time axis is $10/\Gamma_0$. With the above choice of parameters, the fermionic and bosonic

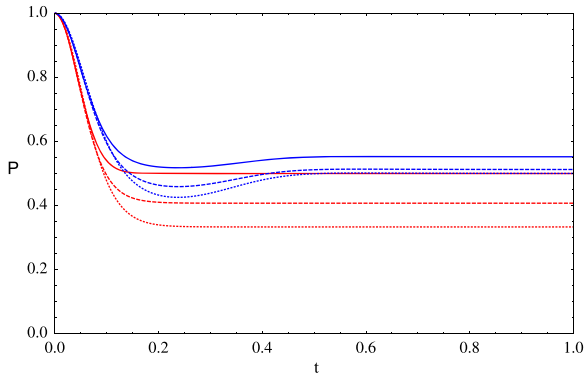

Figure 6. Purity versus t for $\Delta = 2.3$ (red) and $\Delta = 4.1$ (blue) with initial states $|(e_1, e_2, e_3, e_4)\rangle = |(1, 0, 0, 1)\rangle$ (solid), $|(2, 1, 0, 2)\rangle$ (dashed), and $|(1, 1, 0, 1)\rangle$ (dotted).

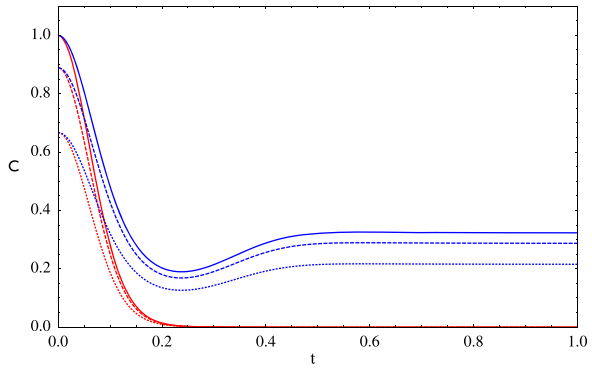

Figure 7. Concurrence versus t for the states and environments specified in figure 6.

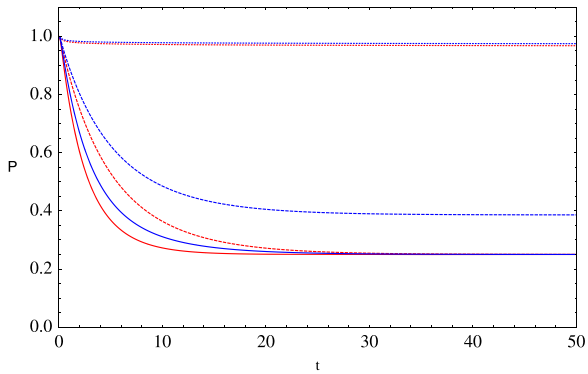

Figure 8. Purity versus t for nonuniform fermionic environments with initial states $|(e_1, e_2, e_3, e_4)\rangle = |(1, 0, 0, 1)\rangle$ (red) and $|(2, 1, 0, 2)\rangle$ (blue). The environments are specified by the κ vector: $(\kappa_1, \kappa_2, \kappa_3, \kappa_4) = (0.5, 0.5, 0.5, 0.5)$ (solid), (0.5, 0.5, 1.2, 1.2) (dashed) and (1.1, 1.1, 2, 2) (dotted).

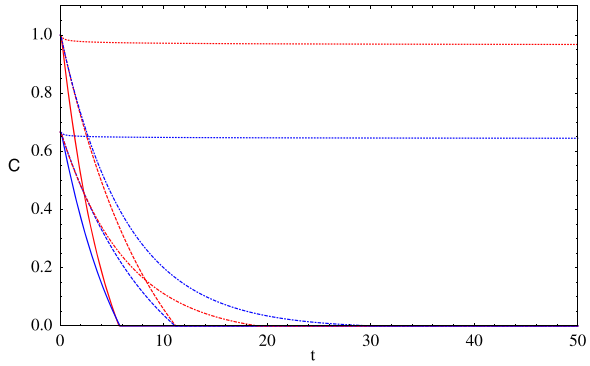

Figure 9. Concurrence versus t for the states and environments specified in figure 8. Here we add the blue and red dot–dashed lines for the initial states $|(e_1, e_2, e_3, e_4)\rangle = |(1, 0, 0, 1)\rangle$ (red) and $|(2, 1, 0, 2)\rangle$ (blue) in the environment with $(\kappa_1, \kappa_2, \kappa_3, \kappa_4) = (0.5, 1.2, 1.2, 0.5)$.

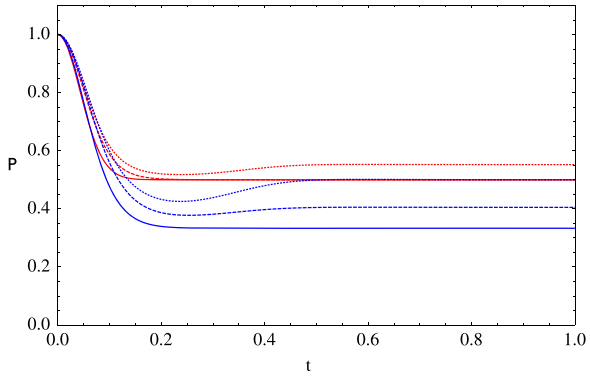

Figure 10. Purity versus t for nonuniform bosonic environments with initial states $|(e_1, e_2, e_3, e_4)\rangle = |(1, 0, 0, 1)\rangle$ (red) and $|(2, 1, 0, 2)\rangle$ (blue). The environments are specified by the Δ vector: $(\Delta_{12}, \Delta_{34}) = (2.3, 2.3)$ (solid), $(2.3, 4.1)$ (dashed) and $(4.1, 4.1)$ (dotted).

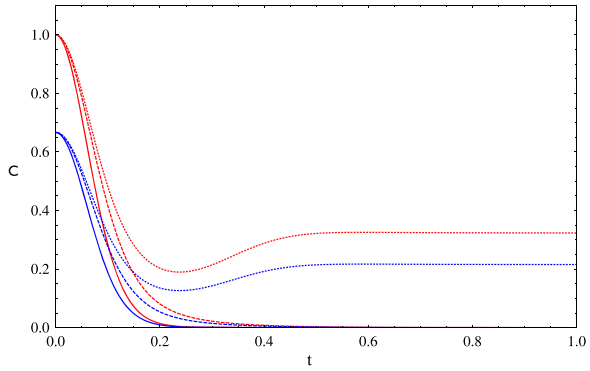

Figure 11. Concurrence versus t for the states and environments specified in figure 10.

environments are on an equal footing, so we can make a comparison of the vulnerabilities of the topological qubits in the two environments for a given initial state.

Figure 4 shows the time evolution of the purity for the uniform fermionic environment with different initial states. Recall that $Q = 2\kappa - 1$, and indeed the plots for $Q > 1$ and $Q \leqslant 1$ behave qualitatively differently. For $Q \leqslant 1$ all the initial states decohere into Gibbs states and thermalize as in the case for a single topological qubit; for $Q > 1$ the initial states first decohere, but then regain some coherence, and finally settle down into some states with purity almost equal to 1. This suggests that the super-Ohmic environment with $Q > 1$ (or $\kappa > 1$, i.e., strongly interacting Luttinger liquids) maintains the purity of the initial states, realizing qubits robust against quantum decoherence.

Similarly, we find, as shown in figure 5, that the patterns of concurrence are different for $Q > 1$ and $Q \leqslant 1$. For $Q \leqslant 1$ the concurrence vanishes around the decoherence time scale given in figure 4; for $Q > 1$, the concurrence drops a little at the beginning and then rises to a final value close to the initial one. The nonzero concurrence for the topological qubits in the super-Ohmic environments ensures that the state remains quantum, even without establishing whether all of the off-diagonal elements of the reduced density matrix diminish or not. Thus, the purity in figure 4 for the $Q > 1$ cases does characterize the quantumness, i.e., the proximity to the initial pure state.

Note that the concurrence pattern shows a converging behavior, i.e., the concurrences of different initial states diminish at almost the same time. This seems to be the case for most of the concurrence plots in this work. However, this is not true generally, as shown by the exceptional black solid line in figure 5. Despite that, as compared to the concurrence patterns of the usual non-topological qubits studied in [44], the patterns here do have the more convergent behaviors.

The time evolution patterns of the purity and concurrence for the uniform bosonic environments are shown in figures 6 and 7, respectively. Recalling that $Q = 2\Delta - 4$, we have plotted in figures 6 and 7 the results for both $Q > 1$ and $Q \leqslant 1$. Comparing to the results in figures 4 and 5 for the fermionic environments, we find two different features. The first is as illustrated in equations (48) and (62): the purity reduces to that for the pointer state but not that for the Gibbs state for $Q \leqslant 1$ cases. The second is that the purity and concurrence for the $Q > 1$ cases settle down to a final nonclassical state value, which is however quite a lot smaller than the initial one for the pure state. This is in contrast to the fermionic case, for which the final value is almost the same as the initial one. Accompanying this is the fact that the decoherence time for the bosonic environments is shorter than that for the fermionic ones.

As our choices of parameters are made for putting fermionic and bosonic environments on an equal footing, we might tempted to infer from the above results that the fermionic environments are more robust in protecting the quantum information of the probe topological qubits than in protecting that of the bosonic ones. This is, in fact, not correct in general. The reason that the decoherence time for the bosonic environment for all of the figures that we have shown is shorter than that for the fermionic one has to do with the prefactors $c_1(\kappa)$ and $c_2(\Delta)$ of the symmetric Green's functions. The analytic expressions for $c_1(\kappa)$ and $c_2(\Delta)$ are respectively shown in equations (C4) and (C6*b*). For the same scaling dimension Q ($Q = 2\kappa - 1$ for the fermionic environment and $Q = 2\Delta - 4$ for the bosonic environment), smaller decoherence time indicates a larger prefactor. In our case, $c_2((Q + 4)/2) > c_1((Q + 1)/2)$ for $Q \geqslant 0.057$ and thus all of the results that we see seem to suggest that the fermionic environment is better at preserving the quantum information (the smallest Q that we show for a bosonic case is 0.6). For

the noninteracting limit, or $Q = 0$, the bosonic environment is actually better at protecting the quantum information, as $c_2(2) < c_1(1/2)$. Thus there is no general rule as to which type of environment is better.

Here we switch gear to studying the effect of the nonuniform environments. As emphasized, this is a peculiar feature for the topological qubits, as their component Majorana modes can be coupled differently to the environment. The nonuniformity of the environment for the two-qubit cases is characterized by the vector of conformal dimensions, i.e., $(\kappa_1, \kappa_2, \kappa_3, \kappa_4)$ (fermionic) and $(\Delta_{12}, \Delta_{34})$ (bosonic), where the subscripts label the corresponding Majorana modes. Note that for the bosonic cases, two Majorana modes labeled a and b couple at the same time to an environmental operator of conformal dimension Δ_{ab}.

Figure 8 shows the time evolution patterns of the purity for nonuniform environments. A peculiarity in this figure is the behavior of the blue dashed line which does not evolve into a Gibbs state like the red dashed line. The blue and red dashed lines are the patterns for the different initial states but in the *same* nonuniform environment. Moreover, one can check that the final state for the blue dashed line is not a pointer state, i.e., the reduced density matrix is not a diagonal matrix. This reflects the fact that the nonuniformity of the environment enhances the breaking of the unitarity of the state space. Thus, some particular subset of states are favored over others for being robust against decoherence.

On the other hand, the time evolution pattern of the concurrence shown in figure 9 does not have this peculiarity, i.e., the blue dashed line has late time vanishing concurrence as the red dotted line does. This is because the concurrence characterizes the quantum entanglement between two topological qubits—e.g., the state $e_1|00\rangle + e_4|11\rangle$ is entangled but $e_1|00\rangle + e_2|01\rangle = |0\rangle(e_1|0\rangle + e_2|1\rangle$ is not—but both are pure states. Moreover, in our setup specified by (54) the first topological qubit is made up of γ_1 and γ_2 and the second one is made up of γ_3 and γ_4. Thus, the nonuniform environment $(\kappa_1, \kappa_2, \kappa_3, \kappa_4) = (0.5, 0.5, 1.2, 1.2)$ can retain the quantum information of the second qubit but not that of the first one. So, this environment may retain the quantumness of the initial state $|(e_1, e_2, e_3, e_4)\rangle = |(2, 1, 0, 2)\rangle$ (the blue dotted line in figure 8, or see appendix F for more discussion) but not its concurrence, as the first topological qubit decoheres into a classical state and can no longer become entangled with the second one. Moreover, for $|(e_1, e_2, e_3, e_4)\rangle = |(2, 1, 0, 2)\rangle$ and $|(1, 0, 0, 1)\rangle$, the amounts of 'useful' information evaluated as the concurrences have equal relative weights (i.e. $e_1 = e_4$) and they are coupled to the same environment. Thus for this case the concurrences diminish at exactly the same time for these two different initial states, as shown by the dashed and solid lines in figure 9.

For general sets of initial states and environment parameters the concurrences need not diminish at the same time; see, e.g., the black solid line in figure 5 or the blue and red dot–dashed lines in figure 9. In particular, for the latter there is an environment with $(\kappa_1, \kappa_2, \kappa_3, \kappa_4) = (0.5, 1.2, 1.2, 0.5)$, which acts on the component Majorana modes of each topological qubit nonuniformly. According to the discussion around equation (50), in this kind of environment the decoherence pattern of the topological qubit is very sensitive to the initial states and should also affect the pattern of concurrence between two topological qubits. This may explain why the red and blue dot–dashed lines (the concurrences for initial states $|(e_1, e_2, e_3, e_4)\rangle = |(1, 0, 0, 1)\rangle$ (red) and $|(2, 1, 0, 2)\rangle$ (blue) in the environment with $(\kappa_1, \kappa_2, \kappa_3, \kappa_4) = (0.5, 1.2, 1.2, 0.5)$, respectively) do not diminish at (almost) the same time, like for the other cases in figure 9.

Similarly, we consider the effect of bosonic nonuniform environments, and the results are shown in figures 10 and 11. Again, as for figure 8, we see a similar enhancement effect of unitarity breaking in figure 10, i.e., the final state purity of the blue dashed line does not merge with that of the blue solid one, which reduces to a pointer state. One can check that the final state of the blue dashed line is not a pointer state. This is in contrast to the merging of the red dashed and solid lines which correspond to another initial state. As for the concurrence, the story is similar to that for the fermionic case: the environment $(\Delta_{12}, \Delta_{34}) = (2.3, 4.1)$ causes complete decoherence of the first topological qubit, so it cannot maintain the quantum entanglement with the second one for the initial state of the blue dashed line.

4. Conclusion

In this paper, we investigate the decoherence patterns of topological qubits made up of Majorana modes weakly coupled to Ohmic-like environments such that the topological properties of Kitaev's chain are preserved. Our results give answers to the following two questions, which motivated our work. The first question is that of whether the topological qubits are robust against decoherence or not. If they are, then the second question is that of in what sense robustness is meant. For the Ohmic-like environments which are mostly considered in the context of quantum decoherence, we find that the topological qubits cannot completely decohere if the environment is super-Ohmic and so is the concurrence (i.e., for quantum entanglement)[10].

Note that the super-Ohmic environments have less spectral density at low energy than the sub-Ohmic ones. Thus naively we expect the qubits to be more robust against decoherence in the super-Ohmic environment, as the low energy degrees of freedom are the main carriers in taking away the quantum information of the probe qubits. Just based on this, however, it is hard to see in what sense robustness is meant, as there is no real mass gap being developed even for a very super-Ohmic spectrum. In fact, the absence of the mass gap leads to complete decoherence of the non-topological qubits in all Ohmic-like environments unless the probe–environment coupling is sufficiently strong [27, 28, 44].

Our results clarify the above issues. Even if there is no gap developed in the super-Ohmic environment, the influence functional equation (49) does develop an effective mass gap imposing a cutoff on the effective carriers such that not all of the quantum information of the topological qubits leaks away. This influence functional is the trademark of topological qubits, contrasting with the one for non-topological qubits; the latter involves also the retarded Green function responsible for the dissipation in the Langevin dynamics of the probe. From our derivation of the open system dynamics, the special form of equation (49) results from the nonlocal nature of the topological qubits and the peculiar algebra of the Majorana modes. The nonlocal nature also requires consideration of the nonuniform environments which cannot be realized for the usual local qubits.

Despite our results shedding new light on the decoherence patterns of the topological qubits in the Ohmic-like environments, we still have not explored all possible situations. For example, we have not considered the interaction Hamiltonian with noncommuting terms. Also, one may consider some more general environments other than Ohmic-like cases, such as the

[10] A type of partial preservation of the topological structure at finite temperature has been reported for topological insulators in [25].

one from the holographic gravity duals in the context of AdS/CFT correspondence as proposed in [40] and studied in [44]. It is also of interest to understand the effect of nonuniform environments in more systematic ways. Finally, reformulating our derivation of the open system dynamics of Majorana modes in the Feynman–Vernon way will definitely shed new light on how to understand our results here, in the context of fluctuation and dissipation of the Langevin dynamics.

Acknowledgments

FLL was supported by Taiwan NSC grants (grant nos 100-2811-M-003-011 and 100-2918-I-003-008). He would also like to thank Yong-Shi Wu and Shi Yu for discussions, and Fudan University and KITPC, where part of the work was done, for hospitality. All of the authors acknowledge support from NCTS.

Appendix A. Schwinger–Keldysh Green functions and the KMS condition

The Schwinger–Keldysh Green functions are the real time two-point functions on the Keldysh contour. They are defined as follows:

$$\begin{aligned} \mathrm{i}G_M^{++}(t-t') &= \left\langle \mathrm{T}\,\mathcal{O}_M(t)\mathcal{O}_M(t')\right\rangle_{\mathcal{E}},\\ \mathrm{i}G_M^{--}(t-t') &= \left\langle \tilde{\mathrm{T}}\,\mathcal{O}_M(t)\mathcal{O}_M(t')\right\rangle_{\mathcal{E}},\\ \mathrm{i}G_M^{+-}(t-t') &= \left\langle \mathcal{O}_M(t)\mathcal{O}_M(t')\right\rangle_{\mathcal{E}},\\ \mathrm{i}G_M^{-+}(t-t') &= \left\langle \mathcal{O}_M(t')\mathcal{O}_M(t)\right\rangle_{\mathcal{E}}, \end{aligned} \tag{A.1}$$

and their relations to the retarded Green function G_{R} and the symmetric Green function G_{sym} are

$$G_R = \frac{1}{2}\left(G^{++} - G^{--} - G^{+-} + G^{-+}\right) \tag{A.2}$$

$$G_{\mathrm{sym}} = \frac{\mathrm{i}}{2}\left(G^{++} + G^{--}\right) = \frac{\mathrm{i}}{2}\left(G^{+-} + G^{-+}\right). \tag{A.3}$$

Moreover, for the thermal environment these two Green functions are related by the Kubo–Martin–Schwinger (KMS) condition [34]:

$$G_{\mathrm{sym}}(\omega) = -[1 \pm 2n(\omega)]\,\mathrm{Im}\,G_R(\omega), \tag{A.4}$$

where the plus sign is for the bosonic channel with $n(\omega) = \frac{1}{\mathrm{e}^{\beta\omega}-1}$, and the minus sign is for the fermionic channel with $n(\omega) = \frac{1}{\mathrm{e}^{\beta\omega}+1}$.

Appendix B. On Gaussian approximation of the influence functional

In this appendix, we compare the explicit expansion in (21) and the one obtained by Gaussian approximation, (23), and show that, up to some overall factor in each order, the two forms behave in qualitatively the same way, i.e., both are just functionals of $\int^t \mathrm{d}\tau \int^t \mathrm{d}\tau'\ \overline{G}_{M,\mathrm{sym}}(\tau-\tau')$ only. Similar structures are also shown for (24).

To start, let us expand $\langle \tilde{\mathrm{T}} \cosh \mathbf{O}_M(t)\, \mathrm{T} \cosh \mathbf{O}_M(t) \rangle_\varepsilon$ directly:

$$\begin{aligned}
&\left\langle \tilde{\mathrm{T}} \cosh \mathbf{O}_M(t)\, \mathrm{T} \cosh \mathbf{O}_M(t) \right\rangle_\varepsilon \\
&= \left(1 + \tfrac{x^2}{2} + \tfrac{x^4}{4!} + \cdots\right)\left(1 + \tfrac{y^2}{2} + \tfrac{y^4}{4!} + \cdots\right) \\
&= 1 + \frac{1}{2}\left(x^2 + y^2\right) + \frac{1}{4!}\left(x^4 + 6x^2y^2 + y^4\right) + \cdots \\
&= 1 + \frac{1}{4}\left((x+y)^2 + (x-y)^2\right) \\
&\quad + \frac{1}{2\cdot 4!}\left((x+y)^4 + (x-y)^4\right) + \cdots,
\end{aligned} \tag{B.1}$$

where

$$\begin{aligned}
x^2 &\equiv \mathrm{i}\int^t \mathrm{d}\tau \int^t \mathrm{d}\tau'\, \overline{G}_M^{++}(\tau - \tau'), \\
y^2 &\equiv \mathrm{i}\int^t \mathrm{d}\tau \int^t \mathrm{d}\tau'\, \overline{G}_M^{--}(\tau - \tau'), \\
xy &\equiv \mathrm{i}\int^t \mathrm{d}\tau \int^t \mathrm{d}\tau'\, \overline{G}_M^{+-}(\tau - \tau') \\
yx &\equiv \mathrm{i}\int^t \mathrm{d}\tau \int^t \mathrm{d}\tau'\, \overline{G}_M^{-+}(\tau - \tau'),
\end{aligned}$$

as defined in (A.1). In the above, the Wick contraction for higher order terms and the symmetrization of xy and yx are assumed.

On the other hand, if we expand the result obtained on the basis of the Gaussian approximation in (23) in the contour basis, this yields

$$\begin{aligned}
&\left\langle \tilde{\mathrm{T}} \cosh \mathbf{O}_M(t)\, \mathrm{T} \cosh \mathbf{O}_M(t) \right\rangle_\varepsilon \approx \tfrac{1}{2}\left(\mathrm{e}^{(x+y)^2/2} + \mathrm{e}^{(x-y)^2/2}\right) \\
&= 1 + \frac{1}{2}\left(x^2 + y^2\right) + \frac{1}{8}\left(x^4 + 6x^2y^2 + y^4\right) + \cdots.
\end{aligned} \tag{B.2}$$

Comparing (B.1) and (B.2), we can see that these two expansions differ by a factor of $(2n-1)!!$ for nth-order terms, i.e., in some sense the exact correlator and its Gaussian approximation are related by a Borel-like sum in the expansion of $(x-y)^2$ and $(x+y)^2$. Note that if we take the Gaussian approximation in another way, e.g., use $\frac{1}{2}(\mathrm{e}^{x^2} + \mathrm{e}^{y^2})$, this will not be related by a Borel-like sum to equation (B.1), although the first-order terms are the same, and will yield incorrect long time behaviors[8].

We should emphasize that this kind of Gaussian approximation is usually adopted in the Feynman–Vernon way of deriving the quadratic form of the influence functional; see e.g. [35, 38]. The difference here is that we have first eliminated the probe field γs by using $\gamma^2 = 1$. Otherwise, our algebraic structures and the Feynman–Vernon one are the same.

The above demonstration shows that, after transforming back to the 'ra' basis, both expressions are order by order just functionals of $\int^t \mathrm{d}\tau \int^t \mathrm{d}\tau'\, \overline{G}_{M,\mathrm{sym}}(\tau - \tau')$, i.e., $(x+y)^2 \equiv 4\int^t \mathrm{d}\tau \int^t \mathrm{d}\tau'\, \overline{G}_{M,\mathrm{sym}}(\tau - \tau')$ and $(x-y)^2 \equiv 0$ by the second equality of equation (A.2). This indicates that the critical behavior that occurred at $Q = 1$ holds

qualitatively to all orders, as the criticality is just encoded in $\int^t \mathrm{d}\tau \int^t \mathrm{d}\tau'\, \overline{G}_{M,\mathrm{sym}}(\tau - \tau')$. Thus, the Gaussian approximation used in this work still ensures the qualitative difference between the sub-Ohmic and super-Ohmic environments when considering the decoherence patterns of the topological qubits. On the other hand, the quantitative difference is the same as for the usual case of Gaussian approximation in the Feynman–Vernon approach, and can be seen as giving the appropriate mean field approximation.

Appendix C. Green functions for the fermionic and bosonic environments

C.1. The fermionic Green function

Here we give the Green function for the fermionic environment considered in the main text. Following [48], the Keldysh components of the bare (uncoupled) zero-temperature helical Luttinger liquid lead Green functions in frequency space are

$$G^{++}_{\psi_{\mathrm{L/R}}}(\omega) = \frac{a_0^{2\kappa}}{2\pi v^{2\kappa}} \frac{\Gamma(\kappa)^2}{\Gamma(2\kappa)} |\omega - \mu|^{2\kappa-1} \left(\tilde{h}(\kappa)\theta(\omega - \mu) - \tilde{h}(\kappa)\theta(\mu - \omega)\right) \tag{C1a}$$

$$G^{--}_{\psi_{\mathrm{L/R}}}(\omega) = \frac{a_0^{2\kappa}}{2\pi v^{2\kappa}} \frac{\Gamma(\kappa)^2}{\Gamma(2\kappa)} |\omega - \mu|^{2\kappa-1} \left(\tilde{h}^*(\kappa)\theta(\mu - \omega) - \tilde{h}^*(\kappa)\theta(\omega - \mu)\right) \tag{C1b}$$

$$G^{+-}_{\psi_{\mathrm{L/R}}}(\omega) = \frac{2\pi a_0^{2\kappa}}{v^{2\kappa}} \frac{\mathrm{i}}{\Gamma(2\kappa)} |\omega - \mu|^{2\kappa-1}\theta(\mu - \omega) \tag{C1c}$$

$$G^{-+}_{\psi_{\mathrm{L/R}}}(\omega) = \frac{2\pi a_0^{2\kappa}}{v^{2\kappa}} \frac{-\mathrm{i}}{\Gamma(2\kappa)} |\omega - \mu|^{2\kappa-1}\theta(\omega - \mu), \tag{C1d}$$

where $\kappa = \frac{1}{4}(K + 1/K)$ and $\tilde{h}(\kappa) = 2\mathrm{e}^{-\mathrm{i}\pi\kappa} \sin(\pi\kappa)\Gamma(1 - \kappa)^2$. $K = 1$ ($\kappa = 1/2$) corresponds to noninteracting fermions and the L/R indices correspond to left/right movers in the one-dimensional system. Notice the relative minus signs in equations (C1*a*) and (C1*b*), due to their fermionic nature.

For our purposes, we have to modify the Green functions in (C1) to 'Majorana-dressed' ones. They are

$$\overline{G}^{++}_{\psi_{\mathrm{L/R}}}(\omega) = \frac{a_0^{2\kappa}}{2\pi v^{2\kappa}} \frac{\Gamma(\kappa)^2}{\Gamma(2\kappa)} |\omega - \mu|^{2\kappa-1} \left(\tilde{h}(\kappa)\theta(\omega - \mu) + \tilde{h}(\kappa)\theta(\mu - \omega)\right) \tag{C2a}$$

$$\overline{G}^{--}_{\psi_{\mathrm{L/R}}}(\omega) = \frac{a_0^{2\kappa}}{2\pi v^{2\kappa}} \frac{\Gamma(\kappa)^2}{\Gamma(2\kappa)} |\omega - \mu|^{2\kappa-1} \left(-\tilde{h}^*(\kappa)\theta(\omega - \mu) - \tilde{h}^*(\kappa)\theta(\mu - \omega) \right) \tag{C2b}$$

$$\overline{G}^{+-}_{\psi_{\mathrm{L/R}}}(\omega) = \frac{2\pi a_0^{2\kappa}}{v^{2\kappa}} \frac{-\mathrm{i}}{\Gamma(2\kappa)} |\omega - \mu|^{2\kappa-1}\theta(\mu - \omega) \tag{C2c}$$

$$\overline{G}^{-+}_{\psi_{\mathrm{L/R}}}(\omega) = \frac{2\pi a_0^{2\kappa}}{v^{2\kappa}} \frac{-\mathrm{i}}{\Gamma(2\kappa)} |\omega - \mu|^{2\kappa-1}\theta(\omega - \mu). \tag{C2d}$$

It is easy to show that the relation between the contour Green functions $\overline{G}^{++} + \overline{G}^{--} = \overline{G}^{+-} + \overline{G}^{-+}$ still holds for these 'Majorana-dressed' Green functions.

Note that in our context, we assume the Majorana zero modes to be coupled locally to the anti-Hermitian operator $\mathcal{O}_a$, as noted in equation (4). Here we assume that $\mathcal{O}_a = \psi_{\mathrm{L/R}} - \psi^\dagger_{\mathrm{L/R}}$, which is anti-Hermitian by construction. Then our symmetric Green function for the operator $\mathcal{O}$ is

$$\begin{aligned}
\overline{G}_{\mathcal{O}_a,\mathrm{sym}}(\omega) &= \frac{\mathrm{i}}{2}\left(\overline{G}^{++}_{\mathcal{O}_a}(\omega) + \overline{G}^{++}_{\mathcal{O}_a}(\omega)\right) \\
&= -\mathrm{i}\left(\overline{G}^{++}_{\psi_{\mathrm{L/R}}}(\omega) + \overline{G}^{--}_{\psi_{\mathrm{L/R}}}(\omega)\right) \\
&= -\frac{a_0^{2\kappa}}{\pi v^{2\kappa}} \frac{\Gamma(\kappa)^2}{\Gamma(2\kappa)} \left(2\mathrm{i}\ \mathrm{Im}\ \tilde{h}(\kappa)\right) |\omega - \mu|^{2\kappa-1} \\
&= c_1(\kappa)\, |\omega - \mu|^{2\kappa-1}.
\end{aligned} \tag{C3}$$

Here we have used Euler's reflection formula $\Gamma(\kappa)^2\Gamma(1-\kappa)^2 \sin^2\pi\kappa = \pi^2$ in going from the second to the third line and defined $c_1(\kappa)$ as

$$c_1(\kappa) \equiv -\frac{4\pi}{\Gamma(2\kappa)} \left(\frac{a_0}{v}\right)^{2\kappa} < 0. \tag{C4}$$

C.2. The bosonic Green function

In the bosonic case, we consider the Green function of a scalar field in AdS_5 space in the long wavelength ($|\vec{k}| \sim 0$) limit such that its Green function effectively reduces to zero dimensions [40, 42]. We denote the dual operator of the scalar by $\mathcal{O}_s$; then its holographic retarded Green function is

$$G_{\mathcal{O}_s,\mathrm{R}}(\omega) = \begin{cases} \dfrac{N_{sc}^2 \Gamma(3-\Delta)\epsilon^{2(\Delta-4)}}{8\pi^2\Gamma(\Delta-2)2^{2\Delta-5}} \left(\omega^2\right)^{\Delta-2} \left[\cos\pi\Delta - \mathrm{i}\ \mathrm{sgn}(\omega) \sin\pi\Delta\right] & 2 < \Delta \notin \mathbb{N} \\ \dfrac{N_{sc}^2 \epsilon^{2(\Delta-4)}}{8\pi^2(\Delta-3)!^2 2^{2\Delta-5}} \left(\omega^2\right)^{\Delta-2} \left[\ln\omega^2 - \mathrm{i}\ \pi\ \mathrm{sgn}(\omega)\right] & 2 \leqslant \Delta \in \mathbb{N}, \end{cases} \tag{C.5}$$

where $N_{\rm sc}^2$ is the number of degrees of freedom of the dual conformal field theory, and $\epsilon \approx 0$ is the UV cutoff of the length scale.

Like for the fermionic case, the bosonic operator $\mathcal{O}_{ab}$ to which the double Majorana modes couple is anti-Hermitian, as noted in equation (4). We then assume that $\mathcal{O}_{ab} = \mathcal{O}_{\rm s} - \mathcal{O}_{\rm s}^{\dagger}$, so $G_{\mathcal{O}_{ab},{\rm R}} = -2G_{\mathcal{O}_{\rm s},{\rm R}}$. Thus, the symmetric Green function of $\mathcal{O}_{ab}$ related to the retarded one (at zero temperature) by equation (A.4) is given by

$$\begin{aligned} G_{\mathcal{O}_{ab},{\rm sym}}(\omega) &= 2\ {\rm sgn}\,(\omega)\ {\rm Im}\ G_{\mathcal{O}_{\rm s},{\rm R}}(\omega) \\ &= c_2(\Delta)\left(\omega^2\right)^{\Delta-2} \end{aligned} \tag{C6a}$$

where

$$c_2(\Delta) \equiv \begin{cases} -\dfrac{N_{\rm sc}^2\Gamma(3-\Delta)\epsilon^{2(\Delta-4)}}{4\pi^2\Gamma(\Delta-2)2^{2\Delta-5}}\ (\sin\pi\Delta) & 2<\Delta\notin\mathbb{N} \\ -\dfrac{N_{\rm sc}^2\epsilon^{2(\Delta-4)}}{4\pi\,(\Delta-3)\,!^2 2^{2\Delta-5}} & 2\leqslant\Delta\in\mathbb{N}. \end{cases} \tag{C6b}$$

Note that for the bosonic channel, $\overline{G}_{\rm sym}(\omega) = G_{\rm sym}(\omega)$.

Appendix D. Purity for a single-qubit system

In this section, we record the explicit form of the purity for a single-qubit system. The explicit forms of the reduced density matrix for fermionic and bosonic environments are given in equations (43) and (44) respectively. It is then straightforward to calculate the purity $\mathcal{P}(t) \equiv {\rm Tr}\,\rho(t)^2$. The explicit forms are given below. For a bosonic environment, the purity takes the form

$$\mathcal{P}^{\rm b}(t) = \frac{1}{N^{\rm b}(t)^2}\Big(a_{01}a_{10}\big(C_{12}+S_{12}\big)^2 + \big(a_{00}^2+a_{11}^2\big)\big(C_{12}-S_{12}\big)^2\Big), \tag{D.1}$$

and

$$\begin{aligned} \mathcal{P}^{\rm f}(t) = \frac{1}{N^{\rm f}(t)^2}\Big(&2\big(a_{01}\big(C_1C_2-S_1S_2\big)+a_{10}\big(C_1S_2-C_2S_1\big)\big) \\ &\times\big(a_{10}\big(C_1C_2-S_1S_2\big)+a_{01}\big(C_1S_2-C_2S_1\big)\big)\Big) \\ &+\frac{1}{N^{\rm f}(t)^2}\Big(\big(a_{11}\big(C_2S_1+C_1S_2\big)-a_{00}\big(C_1C_2+S_1S_2\big)\big)^2 \\ &+\big(a_{00}\big(C_2S_1+C_1S_2\big)-a_{11}\big(C_1C_2+S_1S_2\big)\big)^2\Big) \end{aligned} \tag{D.2}$$

for a fermionic environment. Here $N^{\rm f,b}(t) = {\rm Tr}\,\rho_{\rm r}^{\rm f,\,b}(t)$.

Appendix E. The reduced density matrix for two topological qubits

Here we write down the explicit form for the reduced density matrix of two topological qubits with the initial states given as a superposition of even fermion parity states, i.e.

$\psi(t=0) = a\,|00\rangle + b|11\rangle$ with $|a|^2 + |b|^2 = 1$. The initial density matrix (in the qubit basis $(|00\rangle,\ |01\rangle,\ |10\rangle,\ |11\rangle)^{\mathrm{T}}$) is given in equation (60).

Using equation (20), the nonvanishing reduced density matrix elements $\rho^{\mathrm{f}}_{\mathrm{r},\,ij}(t)$ for the fermionic environmental channel at time t are

$$\mathcal{N}^{\mathrm{f}}(t)\rho^{\mathrm{f}}_{\mathrm{r},\,11}(t) = \big(C_1C_2 + S_1S_2\big)\big(C_3C_4 + S_3S_4\big)\,|a|^2 + \big(C_2S_1 + C_1S_2\big)\big(C_4S_3 + C_3S_4\big)\,|b|^2, \tag{E1a}$$

$$\mathcal{N}^{\mathrm{f}}(t)\rho^{\mathrm{f}}_{\mathrm{r},\,14}(t) = \big(C_1C_2 - S_1S_2\big)\big(C_3C_4 - S_3S_4\big)ab^* - \big(C_2S_1 - C_1S_2\big)\big(C_4S_3 - C_3S_4\big)a^*b = \mathcal{N}(t)\Big(\rho^{\mathrm{f}}_{41}(t)\Big)^*, \tag{E1b}$$

$$\mathcal{N}^{\mathrm{f}}(t)\rho^{\mathrm{f}}_{\mathrm{r},\,22}(t) = -\big(C_1C_2 + S_1S_2\big)\big(C_4S_3 + C_3S_4\big)\,|a|^2 - \big(C_2S_1 + C_1S_2\big)\big(C_3C_4 + S_3S_4\big)\,|b|^2, \tag{E1c}$$

$$\mathcal{N}^{\mathrm{f}}(t)\rho^{\mathrm{f}}_{\mathrm{r},\,23}(t) = \big(C_1C_2 - S_1S_2\big)\big(C_4S_3 - C_3S_4\big)ab^* - \big(C_2S_1 - C_1S_2\big)\big(C_3C_4 - S_3S_4\big)a^*b = \mathcal{N}(t)\Big(\rho^{\mathrm{f}}_{32}(t)\Big)^*, \tag{E1d}$$

$$\mathcal{N}^{\mathrm{f}}(t)\rho^{\mathrm{f}}_{\mathrm{r},\,33}(t) = -\big(C_2S_1 + C_1S_2\big)\big(C_3C_4 + S_3S_4\big)\,|a|^2 - \big(C_1C_2 + S_1S_2\big)\big(C_4S_3 + C_3S_4\big)\,|b|^2, \tag{E1e}$$

$$\mathcal{N}^{\mathrm{f}}(t)\rho^{\mathrm{f}}_{\mathrm{r},\,44}(t) = \big(C_2S_1 + C_1S_2\big)\big(C_4S_3 + C_3S_4\big)\,|a|^2 + \big(C_1C_2 + S_1S_2\big)\big(C_3C_4 + S_3S_4\big)\,|b|^2, \tag{E1f}$$

$$\mathcal{N}^{\mathrm{f}}(t) = \big(C_1 - S_1\big)\big(C_2 - S_2\big)\big(C_3 - S_3\big)\big(C_4 - S_4\big)\Big(|a|^2 + |b|^2\Big). \tag{E1g}$$

Similarly, the nonvanishing elements $\rho^{\mathrm{b}}_{\mathrm{r},\,ij}$ for the bosonic channel are

$$\rho^{\mathrm{b}}_{\mathrm{r},\,11}(t) = \frac{1}{\mathcal{N}^{\mathrm{b}}(t)}\,|a|^2\big(C_{12} - S_{12}\big)\big(C_{34} - S_{34}\big), \tag{E2a}$$

$$\rho^{\mathrm{b}}_{\mathrm{r},\,44}(t) = \frac{1}{\mathcal{N}^{\mathrm{b}}(t)}\,|b|^2\big(C_{12} - S_{12}\big)\big(C_{34} - S_{34}\big), \tag{E2b}$$

$$\rho^{\mathrm{b}}_{\mathrm{r},\,14}(t) = \frac{1}{\mathcal{N}^{\mathrm{b}}(t)}\,a^*b\big(C_{12} + S_{12}\big)\big(C_{34} + S_{34}\big), \tag{E2c}$$

$$\mathcal{N}^{\mathrm{b}}(t) = \Big(|a|^2 + |b|^2\Big)\big(C_{12} - S_{12}\big)\big(C_{34} - S_{34}\big), \tag{E2d}$$

with $(\rho^{\mathrm{b}}_{41}(t)) = (\rho^{\mathrm{b}}_{14}(t))^*$. Note that in this case we only turn on the parity-conserving interactions $\gamma_1\gamma_2\mathcal{O}_{12}$ and $\gamma_3\gamma_4\mathcal{O}_{34}$.

Appendix F. Two topological qubits with a nonuniform fermionic environment

Here we discuss in more detail the effects of nonuniform fermionic environments on two topological qubits, as shown in figures 8 and 9. We choose $(\kappa_1, \kappa_2, \kappa_3, \kappa_4) = (0.5, 0.5, \kappa_0, \kappa_0)$ with $\kappa_0 \gg 1$ (indicating that γ_3 and γ_4 do not leak information into the environments) and the two-qubit bases are chosen as in the main text. To illustrate the physics, we compare the long time behavior for these nonuniform environments with two initial states given by $(e_1, e_2, e_3, e_4) = (1, 0, 0, 1)$ and $(e_1, e_2, e_3, e_4) = (1, 1, 0, 0)$.

For the second choice the initial state is in the form of a product state $(|00\rangle + |01\rangle)$ and the concurrence is zero for all time. For the qubit bases $|ij\rangle$ we expect the information contained in the 'j' qubit not to leak into the environment as $\kappa_0 \gg 1$, but the information contained in the 'i' qubit can leak into the environment as γ_1 and γ_2 are connected with Fermi liquid leads. We expect, from statistical arguments, that at long time the probabilities for $i = 0$ and $i = 1$ should be equal, as these two states are energetically degenerate. Thus for $(e_1, e_2, e_3, e_4) = (1, 0, 0, 1)$ or initial probability 1/2 at $|00\rangle$ and 1/2 at $|11\rangle$, we expect the $|00\rangle$ state to become $|00\rangle$ and $|10\rangle$ with probability 1/4 and the $|11\rangle$ state to become $|01\rangle$ and $|11\rangle$ with probability 1/4. Since the quantum information is carried by the superposition of $|00\rangle$ and $|11\rangle$, dephasing at the first qubit erases this mutual information/memory completely, and the reduced density matrix $\rho_{\rm r}^{{\rm f}(1)}(t)$ at late time becomes

$$\rho_{\rm r}^{{\rm f}(1)}(t \to \infty) = \begin{pmatrix} \frac{1}{4} & 0 & 0 & 0 \\ 0 & \frac{1}{4} & 0 & 0 \\ 0 & 0 & \frac{1}{4} & 0 \\ 0 & 0 & 0 & \frac{1}{4} \end{pmatrix}. \tag{F.1}$$

This is not the case for the second choice of initial state $(e_1, e_2, e_3, e_4) = (1, 1, 0, 0)$, as shown below. Following the same argument as in (1, 0, 0, 1), we expect the $|00\rangle$ state to become $|00\rangle$ and $|10\rangle$ with probability 1/4 and the $|01\rangle$ state to become $|01\rangle$ and $|11\rangle$ with probability 1/4 at late time. The key difference from the (1, 0, 0, 1) case is that the relative phase information for (1, 1, 0, 0) is stored at the second qubit *only*, and the random fluctuations from the first qubit do not influence it. Mathematically speaking, the (1, 1, 0, 0) initial state is $|00\rangle + |01\rangle = |0\rangle \otimes (|0\rangle + |1\rangle)$, and hence the random change on the first qubit (the '$|0\rangle$' state) does not alter the relative phase information $(|0\rangle + |1\rangle)$ of the second qubit. The reduced density matrix $\rho_{\rm r}^{{\rm f}(2)}(t)$ becomes at late time

$$\rho_{\rm r}^{{\rm f}(2)}(t \to \infty) = \begin{pmatrix} \frac{1}{4} & \frac{1}{4} & 0 & 0 \\ \frac{1}{4} & \frac{1}{4} & 0 & 0 \\ 0 & 0 & \frac{1}{4} & \frac{1}{4} \\ 0 & 0 & \frac{1}{4} & \frac{1}{4} \end{pmatrix}. \tag{F.2}$$

We see from equation (F.2) that the reduced density matrix does not go to a pointer state with $(e_1, e_2, e_3, e_4) = (1, 1, 0, 0)$, but it does go to a Gibbs state for (1, 0, 0, 1) in this case. The

physics described in this example explains why we see the different behaviors in figures 8 and 9, and for nonuniformity with some super-Ohmic environment(s) even the fermionic channels do not necessarily go to a Gibbs state.

References

[1] Nayak C, Simon S H, Stern A, Freedman M and Das Sarma S 2008 Non-Abelian anyons and topological quantum computation *Rev. Mod. Phys.* **80** 1083

[2] Wen X-G 1989 Vacuum degeneracy of chiral spin states in compactified space *Phys. Rev.* B **40** 7387
Wen X-G 1990 Topological orders in rigid states *Int. J. Mod. Phys.* B **4** 239
Wen X-G and Niu Q 1990 Ground state degeneracy of the FQH states in presence of random potential and on high genus Riemann surfaces *Phys. Rev.* B **41** 9377

[3] Kitaev A Y 2003 Fault tolerant quantum computation by anyons *Ann. Phys.* **303** 2
Kitaev A Y 2006 Anyons in an exactly solved model and beyond *Ann. Phys.* **321** 2

[4] Levin M and Wen X-G 2005 String-net condensation: a physical mechanism for topological phases *Phys. Rev.* B **71** 045110

[5] Arovas D, Schrieffer J R and Wilczek F 1984 Fractional statistics and the quantum Hall effect *Phys. Rev. Lett.* **53** 722

[6] Alicki R, Fannes M and Horodecki M 2009 On thermalization in Kitaev's 2D model *J. Phys. A: Math. Theor.* **42** 065303

[7] Bombin H, Chhajlany R W, Horodecki M and Martin-Delgado M A 2013 Self-correcting quantum computers *New J. Phys.* **15** 055023

[8] Fu L and Kane C L 2008 Superconducting proximity effect and Majorana fermions at the surface of a topological insulator *Phys. Rev. Lett.* **100** 096407

[9] Hasan M Z and Kane C L 2010 Topological insulators *Rev. Mod. Phys.* **82** 3045

[10] Qi X-L and Zhang S-C 2011 Topological insulators and superconductors *Rev. Mod. Phys.* **83** 1057

[11] Wilczek F 2009 Majorana returns *Nat. Phys.* **5** 614

[12] Arovas D, Schrieffer J R and Wilczek F 1984 Fractional statistics and the quantum hall effect *Phys. Rev. Lett.* **53** 722

[13] Ivanov D A 2001 Non-abelian statistics of half-quantum vortices in p-wave superconductors *Phys. Rev. Lett.* **86** 268

[14] Kitaev A Y 2001 Unpaired Majorana fermions in quantum wires *Phys. Usp.* **44** 131

[15] Sau J D, Lutchyn R M, Tewari S and Sarma S D 2010 Generic new platform for topological quantum computation using semiconductor heterostructures *Phys. Rev. Lett.* **104** 040502

[16] Alicea J 2010 Majorana fermions in a tunable semiconductor device *Phys. Rev.* B **81** 125318

[17] Lutchyn R M, Sau J D and Sarma S D 2010 Majorana Fermions and a topological phase transition in semiconductor-superconductor heterostructures *Phys. Rev. Lett.* **105** 077001

[18] Fidkowski L, Alicea J, Lindner N, Lutchyn R M and Fisher M P A 2012 Universal transport signatures of Majorana fermions in superconductor-Luttinger liquid junctions *Phys. Rev.* B **85** 245121

[19] Wang Z, Liang Q-F, Yao D-X and Hu X Viewing Majorana bound states by rabi oscillations (arXiv:1406.1429)

[20] Sato M, Takahashi Y and Fujimoto S 2009 Non-Abelian topological order in S-wave superfluids of ultracold fermionic atoms *Phys. Rev. Lett.* **103** 020401

[21] Goldstein G and Chamon C 2011 Decay rates for topological memories encoded with Majorana fermions *Phys. Rev.* B **85** 205109

[22] Budich J C, Walter S and Trauzettel B 2012 Failure of protection of Majorana based qubits against decoherence *Phys. Rev.* B **85** 121405

[23] Rainis D and Loss D 2012 Majorana qubit decoherence by quasiparticle poisoning *Phys. Rev.* B **85** 174533
Schmidt M J, Rainis D and Loss D 2012 Decoherence of Majorana qubits by noisy gates *Phys. Rev.* B **86** 085414
[24] Viyuela O, Rivas A and Martin-Delgado M A 2012 Thermal instability of protected end states in a one-dimensional topological insulator *Phys. Rev.* B **86** 155140
[25] Rivas A, Viyuela O and Martin-Delgado M A 2013 Density-matrix Chern insulators: finite-temperature generalization of topological insulators *Phys. Rev.* B **88** 155141
[26] Viyuela O, Rivas A and Martin-Delgado M A 2014 Uhlmann phase as a topological measure for one-dimensional Fermion systems *Phys. Rev. Lett.* **112** 130401
Viyuela O, Rivas A and Martin-Delgado M A 2014 Two-dimensional density-matrix topological fermionic phases: topological Uhlmann numbers *Phys. Rev. Lett.* **113** 076408
[27] Liu H-B, An J-H, Chen C, Tong Q-J, Luo H-G and Oh C H 2013 Anomalous decoherence in a dissipative two-level system *Phys. Rev.* A **87** 052139
[28] Wu S T 2014 Quenched decoherence in qubit dynamics due to strong amplitude-damping noise *Phys. Rev.* A **89** 034301
[29] Schwinger J S 1961 Brownian motion of a quantum oscillator *J. Math. Phys.* **2** 407
[30] Keldysh L V 1964 Diagram technique for nonequilibrium processes *Zh. Eksp. Teor. Fiz.* **47** 1515
Keldysh L V 1965 *Sov. Phys. JETP* **20** 1018
[31] Feynman R P and Vernon F L Jr. 1963 The theory of a general quantum system interacting with a linear dissipative system *Ann. Phys.* **24** 118
Feynman R P and Vernon F L Jr. 2000 *Ann. Phys.* **281** 547
[32] Caldeira A O and Leggett A J 1983 Path integral approach to quantum Brownian motion *Physica* A **121** 587
[33] Grabert H, Schramm P and Ingold G L 1988 Quantum Brownian motion: the functional integral approach *Phys. Rep.* **168** 115
[34] Kubo R 1957 Statistical mechanical theory of irreversible processes. 1. General theory and simple applications in magnetic and conduction problems *J. Phys. Soc. Jap.* **12** 570
Martin P C and Schwinger J S 1959 Theory of many particle systems. 1 *Phys. Rev.* **115** 1342
[35] Hu B L, Paz J P and Zhang Y-h 1992 Quantum Brownian motion in a general environment: 1. exact master equation with nonlocal dissipation and colored noise *Phys. Rev.* D **45** 2843
[36] Su Z-B, Chen L-Y, Yu X-T and Chou K-C 1988 Influence functional and closed-time-path Green's function *Phys. Rev.* B **37** 9810
[37] Chou K-c, Su Z-b, Hao B-l and Yu L 1985 Equilibrium and nonequilibrium formalisms made unified *Phys. Rep.* **118** 1
[38] Boyanovsky D, Davey K and Ho C M 2005 Particle abundance in a thermal plasma: quantum kinetics vs. Boltzmann equation *Phys. Rev.* D **71** 023523
[39] Son D T and Teaney D 2009 Thermal noise and stochastic strings in AdS/CFT *J. High Energy Phys.* JHEP07(2009)021
[40] Ho S-H, Li W, Lin F-L and Ning B 2014 Quantum decoherence with holography *J. High Energy Phys.* JHEP01(2014)170
[41] Liu H and Suh S J 2014 Entanglement tsunami: universal scaling in holographic thermalization *Phys. Rev. Lett.* **112** 011601
[42] Son D T and Starinets A O 2002 Minkowski space correlators in AdS / CFT correspondence: recipe and applications *J. High Energy Phys.* JHEP09(2002)042
[43] Tu M W-Y and Zhang W-M 2008 Non-Markovian decoherence theory for a double-dot charge qubit *Phys. Rev.* B **78** 235311
Jin J S, Tu M W-Y, Zhang W-M and Yan Y J 2010 Non-equilibrium quantum theory for nanodevices based on the FeynmanVernon influence functional *New J. Phys.* **12** 083013
[44] Chen J H, Ho S H, Lin F L and Liu P H work in progress

[45] Zhang W-M, Lo P-Y, Xiong H-N, Tu M W-Y and Nori F 2012 General non-Markovian dynamics of open quantum systems *Phys. Rev. Lett.* **109** 170402
[46] König M, Wiedmann S, Brüne C, Roth A, Buhmann H, Molenkamp L W, Qi X-L and Zhang S-C 2007 *Science* **318** 766
[47] Kane C L and Fisher M P A 1992 Transport in a one-channel Luttinger liquid *Phys. Rev. Lett.* **68** 1220
[48] Chao S-P, Silotri S A and Chung C-H 2013 Nonequilibrium transport of helical Luttinger liquids through a quantum dot *Phys. Rev.* B **88** 085109
[49] Gogolin A O, Nersesyan A A and Tsvelik A M 2004 *Bosonization and Strongly Correlated System* (Cambridge: Cambridge University Press)
[50] Ryu S, Moore J E and Ludwig A W W 2012 Electromagnetic and gravitational responses and anomalies in topological insulators and superconductors *Phys. Rev.* B **85** 045104
[51] Haehl F M, Loganayagam R and Rangamani M 2014 *J. High Energy Phys.* JHEP03(2014)034
[52] Zurek W H 1981 Pointer basis of quantum apparatus: into what mixture does the wave packet collapse? *Phys. Rev.* D **24** 1516
Zurek W H 1982 Environment induced superselection rules *Phys. Rev.* D **26** 1862
Zurek W 1993 Preferred states predictability classicality and the environment-induced decoherence *Prog. Theor. Phys.* **89** 281
[53] Hill S and Wootters W K 1997 Entanglement of a pair of quantum bits *Phys. Rev. Lett.* **78** 5022
Wootters W K 1998 Entanglement of a pair of quantum bits *Phys. Rev. Lett.* **80** 2245